communications biology

A Nature Portfolio journal

Article

https://doi.org/10.1038/s42003-025-07709-5

Transcriptional dynamics in type 2 diabetes progression is linked with circadian, thermogenic, and cellular stress in human adipose tissue

Irais Rivera-Alvarez[1], Rosa Vázquez-Lizárraga[1,2], Lucía Mendoza-Viveros[1,9], Israim Sotelo-Rivera[1], Tannia L. Viveros-Ruiz[3], Jesús Morales-Maza[4], Lorena Orozco[1], Marta C. Romano[5], Lilia G. Noriega[6], Armando R. Tovar[6], Lorena Aguilar-Arnal[7], Ivette Cruz-Bautista[3], Carlos Aguilar-Salinas[3,8] & Ricardo Orozco-Solis[1,2] ✉

The prevalence of type 2 diabetes (T2D) has increased significantly over the past three decades, with an estimated 30–40% of cases remaining undiagnosed. Brown and beige adipose tissues are known for their remarkable catabolic capacity, and their ability to diminish blood glucose plasma concentration. Beige adipose tissue can be differentiated from adipose-derived stem cells or through transdifferentiation from white adipocytes. However, the impact of T2D progression on beige adipocytes' functional capacity remains unclear. Transcriptomic profiling of subcutaneous adipose tissue biopsies from healthy normal-weight, obese, prediabetic obese, and obese subjects diagnosed with T2D, reveals a progressive alteration in cellular processes associated with catabolic metabolism, circadian rhythms, thermogenesis-related signaling pathways, cellular stress, and inflammation. MAX is a potential transcription factor that links inflammation with the circadian clock and thermogenesis during the progression of T2D. This study unveils an unrecognized transcriptional circuit that increasingly disrupts subcutaneous adipose tissue oxidative capacity during the progression of T2D. These findings could open new research venues for developing chrono-pharmaceutical strategies to treat and prevent T2D.

According to the World Health Organization (WHO) and the Pan American Health Organization, the prevalence of diabetes has increased dramatically worldwide over the past three decades[1]. It is estimated that about 30–40% of cases are undiagnosed, with a projected increase of approximately 50% by 2045, reaching nearly 697 million people with diabetes[2]. Type 2 diabetes (T2D) is a complex disease involving various tissues and organs, with genetic, aging, and environmental factors, such as socioeconomic status, nutrition, sedentary lifestyle, sleep disturbances, and circadian derangements playing significant roles[3]. Overweight and obesity, are closely associated with the development of T2D[4]. However, not all individuals with a positive energy balance, overweight, or obesity develop T2D, implying the existence of cellular and physiological mechanisms that protect certain individuals with a high body mass index (BMI) (> 25 kg/m^2) from T2D development.

Adipose tissue, plays a critical role in endocrine and metabolic regulation, influencing the function of targeted organs such as muscle, liver,

[1]Instituto Nacional de Medicina Genómica (INMEGEN), México City, México. [2]Centro de Investigación sobre el Envejecimiento, Centro de Investigación y de Estudios Avanzados (CIE-CINVESTAV), México City, México. [3]Unidad de Investigación de Enfermedades Metabólicas, Instituto Nacional de Ciencias Médicas y Nutrición Salvador Zubirán (INCMNSZ), México City, México. [4]Departamento de Cirugía Endocrina, Instituto Nacional de Ciencias Médicas y Nutrición Salvador Zubirán (INCMNSZ), México City, México. [5]Departamento de Fisiología, Biofísica y Neurociencias, Centro de Investigación y Estudios Avanzados (CINVESTAV), México City, México. [6]Departamento de Fisiología de la Nutrición, Instituto Nacional de Ciencias Médicas y Nutrición Salvador Zubirán (INCMNSZ), México City, México. [7]Instituto de Investigaciones Biomédicas, Universidad Nacional Autónoma de México (UNAM), México City, México. [8]Escuela de Medicina y Ciencias de la Salud, Tecnológico de Monterrey, México City, México. [9]Present address: División de Biología Molecular, Instituto Potosino de Investigación Científica y Tecnológica, San Luis Potosi, S.L.P., México. ✉e-mail: drorozcos@inmegen.gob.mx

pancreas, and brain through the secretion of adipokines and activated lipids[4,5], which contributes to the control of the whole-body glucose homeostasis. Humans have three major types of adipose tissue: white adipose tissue (WAT), brown adipose tissue (BAT), and beige adipose tissue (beige AT). BAT and beige AT share functional and microstructural features, such as higher mitochondrial content and catabolic capacity, transforming chemical energy into heat, compared to WAT.

Notably, in both rodents and humans, BAT activity has been inversely correlated with plasmatic glucose levels[6–10]. Acute cold stimulation or BAT transplantation from humans and mice can enhance glucose uptake in BAT, leading to an improved glucose metabolism and insulin sensitivity in rodent models[11]. Although BAT and beige AT share several functional properties, they differentiate from distinctive stem cell lineages. While WAT and beige AT predominantly differentiate from adipocytic lineages, BAT differentiates from a myogenic lineage[12]. Beige adipocytes can also arise through the transdifferentiation of white adipocytes, a process known as "browning" of WAT, while the inverse process is known as "whitening"[13]. Remarkably, subcutaneous adipose tissue (SAT) exhibits a greater propensity for browning compared to visceral adipose tissue (VAT) due to its predominantly smaller size and higher density of sympathetic nerves and blood vessels, crucial for regulating thermogenesis and browning. Furthermore, there are contrasting patterns of browning gene expression in VAT and SAT depots between humans and mice, with humans displaying elevated expression of browning genes on SAT and mice exhibiting higher expression in VAT[14]. As a result, the stimulation of brown and beige adipose tissue in vivo has garnered considerable interest for its potential in treating both T2D and obesity[10,15,16].

Nevertheless, current treatments, such as acute cold exposure, β3-agonists like mirabegron, or adipose tissue modulators like thiazolidinediones (TZDs), are challenging in a long term due to discomfort or side effects, including cardiovascular overstimulation, weight gain, fluid retention, bone loss, and heart problems[17,18]. Consequently, there is a need for new strategies to induce browning in vivo, considering its potential therapeutic benefits for T2D and obesity[10,15,16].

To gain insights into the functionality of beige adipocytes during the progression of T2D, we conducted an unbiased transcriptomic analysis of SAT obtained from normal-weight (NW) subjects, patients diagnosed with overweight/obesity (OW), OW subjects diagnosed with pre-diabetes (PD), and OW patients diagnosed with T2D (Supplementary Table 1). Additionally, we complemented the analysis by measuring the cellular oxygen consumption rate (OCR) in differentiated beige adipocytes cultures obtained from the corresponding isolated adipose-derived stem cells (ASCs) from SAT in the different experimental groups. Our results revealed a progressive alteration in gene expression from OW and PD towards the development of T2D. This alteration forms a molecular syndrome involving disrupted cellular processes, including circadian rhythms, oxidative and catabolic capacity, cellular integrity, and inflammation. Ultimately, these changes contribute to the reduction of the thermogenic capacity of adipocytes.

Results

Subcutaneous adipose tissue undergoes progressive transcriptional alterations during the progression of T2D

The SAT plays a crucial role in the pathophysiology of T2D. Thus, our objective was to identify potential molecular mechanisms altered during the progression of T2D in this tissue. Initially, we classified the samples based on clinical parameters (Supplementary Table 1). T2D group exhibited higher values in glucose metabolic parameters, including fasting blood glucose and glycosylated hemoglobin compared to other groups. Notably, insulin levels did not differ between the PD group and the OW or the T2D group; as expected, fasting glucose is under normal parameters, in the NW and OW groups (Supplementary Table 1).

Subsequently, our goal was to identify transcriptional signatures that may occur during the disease progression. We reasoned that, by comparing NW vs. each of the other groups, we could distinguish early (OW vs. NW), intermediate (PD vs. NW), and late (T2D vs. NW) transcriptional signatures reflecting functional adaptations. These signatures were noted as Stage 1–3 (S1-3) respectively (Fig. 1a). Interestingly, the number of

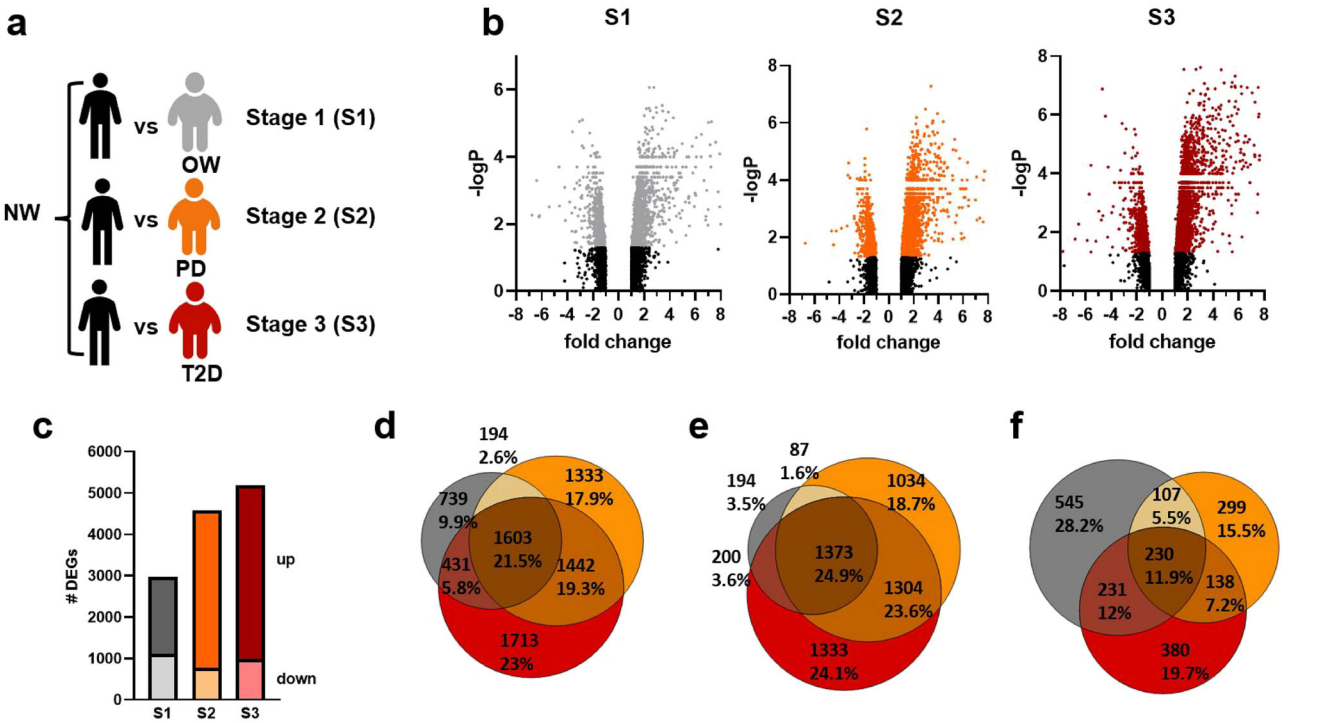

Fig. 1 | Transcriptional alterations occur during the progression of T2D. **a** Normal-weight individuals (NW) ($n = 7$) were compared with overweight/obese (OW) individuals (S1) ($n = 8$), OW with prediabetes (PD) (S2) ($n = 7$), and OW with type 2 diabetes (T2D) (S3) ($n = 8$). **b-c** Volcano plots depict the identified DEGs in each stage and the number of up- or down-regulated DEGs in OW (S1), PD (S2), and T2D (S3), ($P < 0.05$, |log2(Fold Change)|>1.1). **d–f** Venn diagrams illustrate shared and exclusive DEGs in each stage.

differentially expressed genes (DEGs) identified in each comparison progressively increased from 2,967 in S1 to 4,572 in S2 and 5,189 in S3 (Fig. 1b, c). While up-regulated DEGs showed the highest proportion of common genes in all stages (24.9%), only a limited number were exclusively upregulated in S1 (3.5%). However, in S2 and S3, this number was much higher for both exclusively upregulated genes and those shared between these stages (Fig. 1e). In contrast, down-regulated genes exhibited more heterogeneous proportions between the three stages (Fig. 1f).

Given the established sexual dimorphism in various aspects of T2D, including diagnosis, prevention, and treatment[19,20], we aimed to investigate whether the identified DEGs would be influenced by sex (Supplementary Table 2). As anticipated, the factor analysis of mixed data (FAMD) revealed that at stages S1, S2, and S3, the sample distribution was grouped by diagnosis, with NW and OW individuals positioned in distinct quadrants (Supplementary Fig. 1a–c). However, the sex distribution did not exhibit a significant separation between diagnoses (Supplementary Fig. 1d–f), suggesting that within the analyzed DEGs, sex may not have a substantial influence on the observed patterns in these samples.

To gain insights into the altered biological processes during the disease progression, we first analyzed the upregulated DEGs for functional enrichment. As expected, the commonly upregulated DEGs among the three groups (OW, PD, and T2D) are highly enriched in processes related to immune responses, including the adaptive immune system, inflammatory response, and tumor necrosis factor production, among others (Supplementary Fig. 2). Indeed, it has been widely reported that there is transcriptional induction of genes related to inflammation and immune processes in metabolic-related diseases in adipocytes[21,22]. Interestingly, in the S3 group, we found functions related to epigenetic mechanisms, including histone acetyltransferases (HATs), acetylation and deacetylation of histones, response to glucose, and NOTCH signaling. To gain additional insight into histone-modification enzymes, we constructed a protein-protein interactome network using several histone-modifying enzymes, (Supplementary Fig. 3a, b). We identified histone deacetylase 4 and 11 (*HDAC4, 11*), the histone methyltransferase complex regulatory subunit DPY30, and the histone H2A variant Y (*H2AY*) and the chromatin regulator ASF1A, whose expression was upregulated during the progression of T2D. (Supplementary Fig. 3c–g). In this context, the upregulation of these chromatin remodelers had been linked to metabolic control, and cellular stress and senescence[23–30].

Downregulation of catabolic and thermogenic genes during the development of T2D

Since we observed a relatively lower proportion of shared genes between S2 and S3 groups among the down-regulated genes (Fig. 1f), we focused our analysis on these, which may reflect the loss of function in specific processes during the progression of the disease. Strikingly, our analysis revealed an over-representation of rhythmic processes and circadian rhythm genes in all three stages (Fig. 2a). Additionally, crucial pathways such as angiogenesis, the insulin signaling pathway, transcription factors in adipogenesis, calcium signaling pathway, and cAMP signaling pathway were consistently downregulated across all stages, with a more pronounced effect observed in the PD and T2D groups (Fig. 2a).

Upon closer examination of exclusively differentially expressed genes (DEGs) in each stage, S1 exhibited notable enrichment in pathways such as adrenergic receptor signaling, thyroid stimulating hormone, VEGF ligand-receptor, and mRNA processing (Fig. 2b). In S2, the insulin signaling and MAPK signaling pathways were revealed (Fig. 2c). Notably, S3 showed an increased number of downregulated pathways related to cellular metabolism, (Fig. 2d). These included sterol regulatory element-binding proteins, PI3K-AKT-mTOR signaling, and hormone signaling (glucagon, insulin, estrogen, and leptin pathways). Significantly, a decrease in fatty acid metabolism-related transcripts, encompassing processes like fatty acid metabolic and catabolic processes, fatty acid oxidation, and beta-oxidation, were observed. Genes associated with thermogenesis, particularly positive regulation of cold-induced thermogenesis, were downregulated at this stage (Fig. 2d). Notably, genes regulating circadian rhythms were once again identified, consistent with their higher representation in shared DEGs (Fig. 2a, d).

Next, we sought to explore functional evidence for these identified metabolic processes. We constructed a protein-protein interaction network by analyzing the downregulated DEGs participating in the identified processes (Fig. 2d). Interestingly, this analysis predicted the interaction of 86 proteins (Supplementary Fig. 4a), participating in key pathways controlling metabolism, including circadian rhythms, lipid metabolic processes, PI3K-AKT signaling, thyroid-stimulating hormone signaling, AMPK signaling, insulin signaling, cAMP signaling, FoxO2 signaling, glucagon signaling pathway, thermogenesis, and positive regulation of cold-induced thermogenesis, among others (Supplementary Fig. 4b). Importantly, correlation analysis between the expression levels of genes coding for the interacting proteins and clinical parameters related to glucose metabolism including, blood glucose, insulin, HbA1c among others, revealed an increase in the number of significant correlations as the disease progresses (Supplementary Fig. 5, Supplementary Data 2).

These results support the notion that, in the later stages of T2D progression, the catabolic capacity of beige adipocytes is compromised. To further assess this, we employed both BATLAS and ProFat computational tools to predict the degree of beiging within each SAT sample[31,32]. Strikingly, both methods revealed a reduced beiging capacity in the T2D group (Supplementary Fig. 6a, b). Accordingly, a slight reduction of protein levels of the sympathetic nerve marker tyrosine hydroxylase (TH) was observed (Fig. 2e), suggesting decreased sympathetic innervation in the PD and T2D groups[33–35].

Collectively, these results suggest that during the progression of T2D, an increasing number of genes undergo transcriptional alterations, with a notorious reduction in the expression of genes participating in key catabolic processes.

Mitochondrial function is altered during the T2D progression in beige adipocytes

Our results demonstrate that, during the progression of T2D, an increasing number of genes involved in cellular pathways related to lipid catabolism, the thermogenic pathway, and beiging undergo transcriptional alterations (Figs. 1c, 2d, Supplementary Fig. 6a, b). Additionally, mitochondrial dysfunction and content have been associated with insulin resistance, T2D, and obesity[36,37]. This organelle plays a pivotal role in the induction of thermogenesis in both brown and beige adipose tissues. In line with this, the relative mitochondrial content in biopsies showed a gradual reduction in mtDNA content (Fig. 3a), supporting the notion that cellular oxidative capacity is compromised during the progression of T2D.

To directly test this possibility, we quantified cellular oxidative capacity and calculated several bioenergetic parameters. Adipose-derived stem cells (ASCs) were isolated from SAT biopsies and were differentiated to beige adipocytes. To corroborate the differentiation towards beige adipocytes, we also differentiated ASCs into white adipocytes and compared the relative mitochondrial content[38]. Differentiated beige adipocytes exhibited a higher relative mitochondrial DNA content compared to the differentiated white adipocytes and to SAT biopsies, confirming successful stimulation of the thermogenic program (Supplementary Fig. 7a, b)[38].

By measuring the oxygen consumption rate (OCR) in beige cultures from all groups, we found that basal respiration significantly decreased in the PD and T2D groups compared with the NW or OW groups (Fig. 3b, Supplementary Fig. 7c), indicating reduced oxidative capacity. This alteration may reflect an overall disturbance in cellular and mitochondrial energetics. Strikingly, we observed a substantial decrease in proton leak and coupling efficiency (Fig. 3c, d, i), implying a reduction in mitochondrial activity in these groups. Additionally, the glycolytic component of metabolic capacity was also altered, showing a reduced glycolytic capacity in the metabolically compromised PD and T2D groups (Fig. 3g), likely linked with reduced insulin sensitivity, as observed in skeletal muscle[39].

To identify metabolic phenotypes, we compared proton leak versus coupling efficiency (Fig. 3i). Metabolically healthy cohorts (NW and OW)

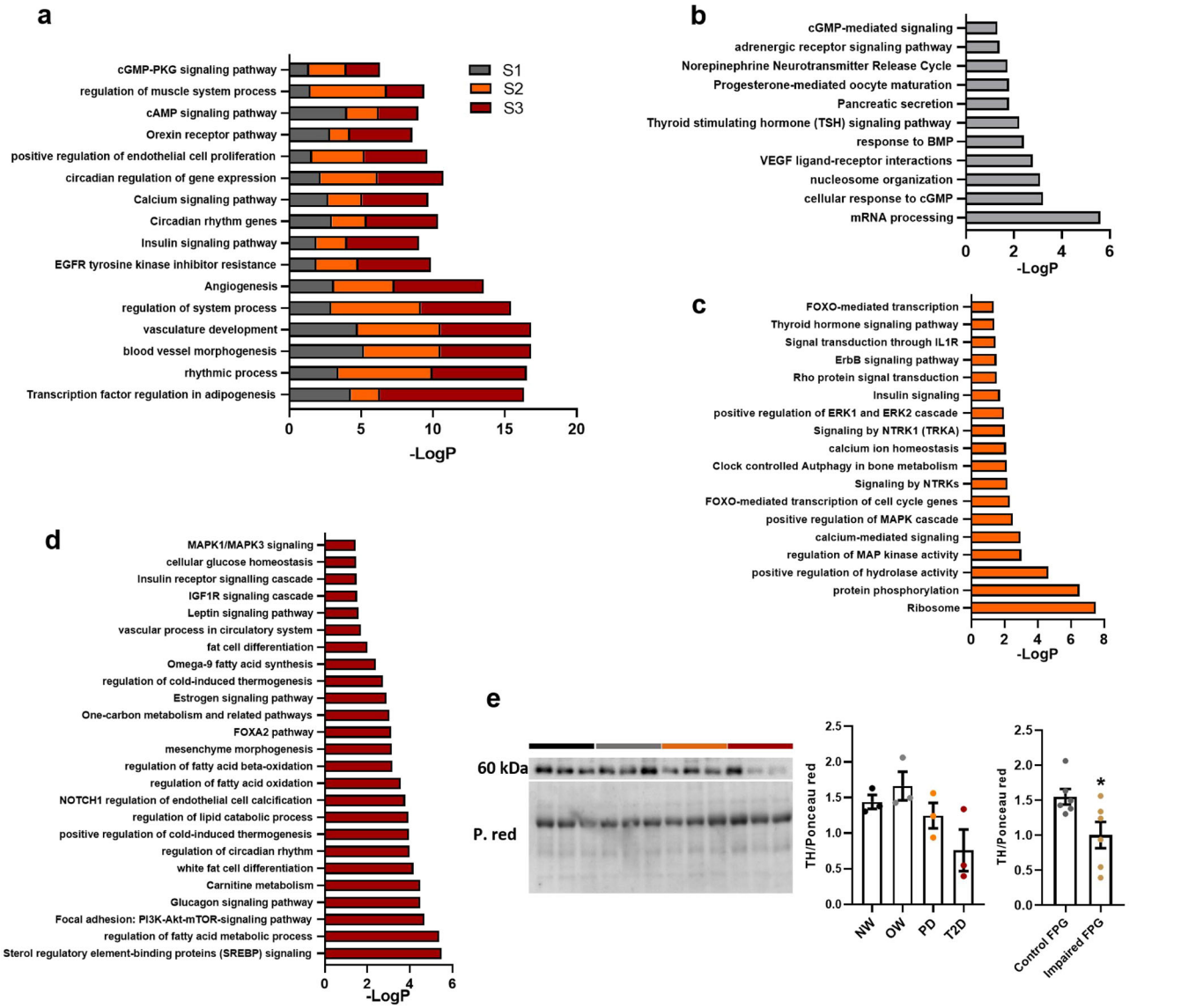

Fig. 2 | Catabolic and thermogenic genes are downregulated during the progression of T2D. a-d Significantly enriched biological functions in each stage, from the down-regulated DEGs ($P < 0.05$, |log2(Fold Change)|>1.1) in S1 (OW), S2 (PD), and S3 (T2D). **e** Tyrosine hydroxylase (TH) protein levels on SAT from NW (black), OW (gray), PD (orange), and T2D (red) individuals; TH protein levels bar graph, one-way ANOVA followed by Tukey´s post-hoc test ($n = 3$). TH protein levels on SAT from control (dark gray) and Impaired Fasting Plasma Glucose (FPG) (dark gold) individuals, t-test (*$P < 0.05$) ($n = 6$). Error bars as mean ± SEM.

fell into the top right corner of the diagram, reflecting a higher catabolic capacity and ATP synthesis. Conversely, the metabolically compromised groups were distributed into the lower left corner, showing lower proton leak and coupling efficiency. A similar profile was observed with glycolytic capacity (Fig. 3j), indicating a reduction in carbohydrate utilization to produce heat (presumably by proton leak) in the samples from metabolically compromised cohorts.

We further calculated the spare respiratory capacity (SRC) and bioenergetic health index (BHI), two indicators of cellular functionality[40,41]. SRC, an indicator of metabolic flexibility, has been inversely related to browning in adipocytes from obese individuals and to plasma glucose levels in obese subjects[42,43]. We found a reduced SRC in the PD and T2D groups (Fig. 3e, k). Similarly, lower values of BHI were observed in these groups (Fig. 3f, k), indicating that beige adipocytes from metabolically unhealthy individuals display reduced mitochondrial function and oxidative capacity. Indeed, BHI has been identified to be lower in peripheral blood cells from patients with T2D and nephropathy compared to those with non-complications[44] and is positively related to fasting insulin sensitivity[45].

When measuring the relative mitochondrial DNA content in differentiated beige adipocytes, no differences were found (Fig. 3h), under probeiging culture conditions. This finding suggests that mitochondrial dysfunction prominently contributes to the reduction in oxidative capacity during the progression of T2D.

The circadian clock is progressively altered during the progression of T2D

Given that the term "biological rhythm" emerged as the most represented process in the interactome from the downregulated DEGs in the S3 (Supplementary Fig. 4b), we assessed the number of known circadian-expressed genes according to adipose tissue from human and mouse databases[46]. We found that 4.6% and 18.4% of the interacting genes to be expressed in a circadian manner in human and mouse adipose tissues, respectively (Supplementary Fig. 4c, Supplementary Data 2). However, when considering various tissues from post-mortem human adipose tissue and mice adipose tissue we found that 95% of the interacting genes (Supplementary Fig. 4d, Supplementary Data 2) were indeed expressed in a circadian manner

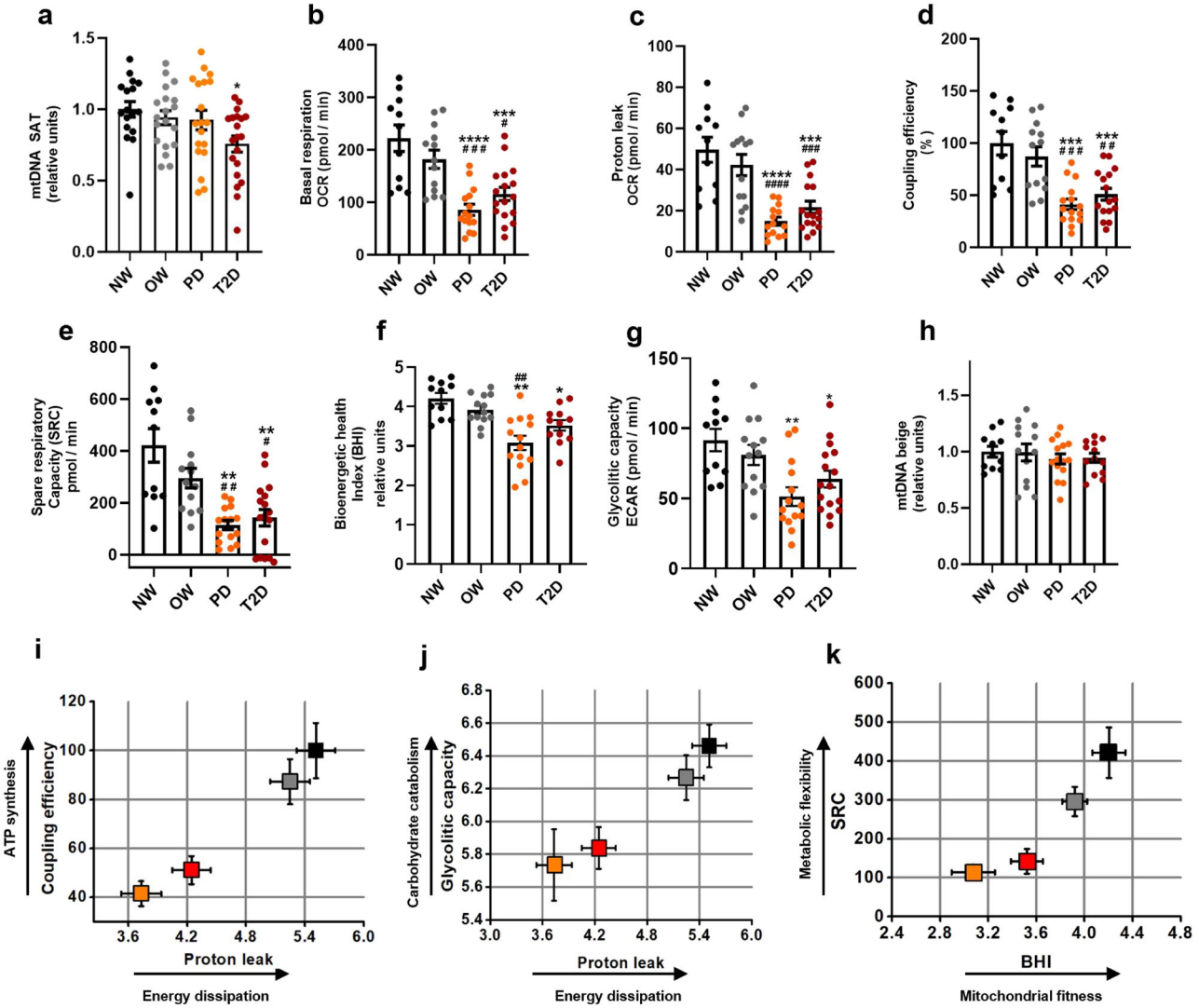

Fig. 3 | Respiratory capacity is impaired in beige adipocytes during the progression of T2D. a Relative mitochondrial DNA content in SAT, NW ($n = 17$), OW ($n = 19$), PD ($n = 19$), T2D ($n = 22$), independent samples. **b** Basal respiration, **c** Proton leak, **d** Coupling efficiency, **e** Spare respiratory capacity (SRC), **f** Bioenergetic health index (BHI), **g** Glycolytic capacity. NW ($n = 11$), OW ($n = 13$), PD ($n = 16$), T2D ($n = 17$), **h** Relative mitochondrial DNA content in differentiated beige adipocyte NW ($n = 12$), OW ($n = 14$), PD ($n = 16$), T2D ($n = 16$), independent samples. One-way ANOVA followed by Tukey's post-hoc test (**a-d, h**), Kruskal-Wallis with Dunn´s (**g**), One way ANOVA with Welch´s correction followed by Dunnett´s T3 (**f**) and Welch ANOVA with Dunnett's T3 (**e**). Significant difference vs. NW group $^{*}P < 0.05$, $^{**}P < 0.01$, $^{***}P < 0.001$, $^{****}P < 0.0001$. Significant difference vs. OW group #P < 0.05, ##$P < 0.01$, ###$P < 0.001$, ####$P < 0.0001$. **i-k** Bioenergetic phenotype, NW ($n = 11$), OW ($n = 13$), PD ($n = 16$), T2D ($n = 17$). Error bars as mean ± SEM.

($P < 0.05$, JTK-P)[47], this suggests that the circadian clock may play a significant role in the rhythmic expression of these genes.

To gain insights into the circadian clock function in each group, we compared the expression of some clock-controlled genes (CCGs) in each stage. Some genes were observed to be either upregulated or downregulated across the three stages (Fig. 4a, b).

Assuming that the conserved transcriptional-translational feedback loop mechanism controlling the circadian expression of core-clock genes (CoCGs) which is the first layer of transcriptional regulation for thousands of CCGs[48], we hypothesized that the expression level between CoCGs should preserve a specific expression relation at each time of the day[49]. Since the biopsies were collected in a narrow timeframe (7:00–8:00 h.), we calculated the ratio between the expression of different pairs of core-clock genes. We selected two sets of core-clock genes known to be expressed in antiphase: *ARNTL, CLOCK, NFIL3, NPAS1, NPAS3* as "Phase" genes and *BHLHE40, BHLHE41, CRY1, CRY2, DBP, NR1D1, NR1D2, PER1, PER2* as "Antiphase" genes[50] (Fig. 4c, Supplementary Fig. 8n-p). In line with the enrichment of circadian-related genes (Fig. 2a, d, Supplementary Fig. 4b), we observed a progressive effect across the different groups. This effect was inverse between antiphase genes as demonstrated by the *PER2* and *CLOCK* ratios (Fig. 4d, e, Supplementary Fig. 8a–m).

Indeed, the correlation analysis between the ratio values and the blood glucose or HA1Ab parameters, show that the absolute values (abs) or ratios values obtained from genes with similar acrophase (phase:phase or antiphase:antiphase) such as *CLOCK:ARNTL* or *CLOCK:NPAS3*, or *PER2:PER1* and *PER2:CRY2* gene pairs, displayed significantly fewer correlations than those obtained from phase-antiphase gene ratios (Fig. 4f, g, Supplementary Fig. 9, 10). This finding highlights a progressive effect on the different groups, suggesting that disruptions in the circadian clock during disease progression—specifically, the expression patterns of antiphase core-clock genes—may reflect a progressive alteration of the circadian clock associated with disease development. This supports the notion that obesity-related metabolic changes are closely tied to alterations in the main core-clock genes[51–56].

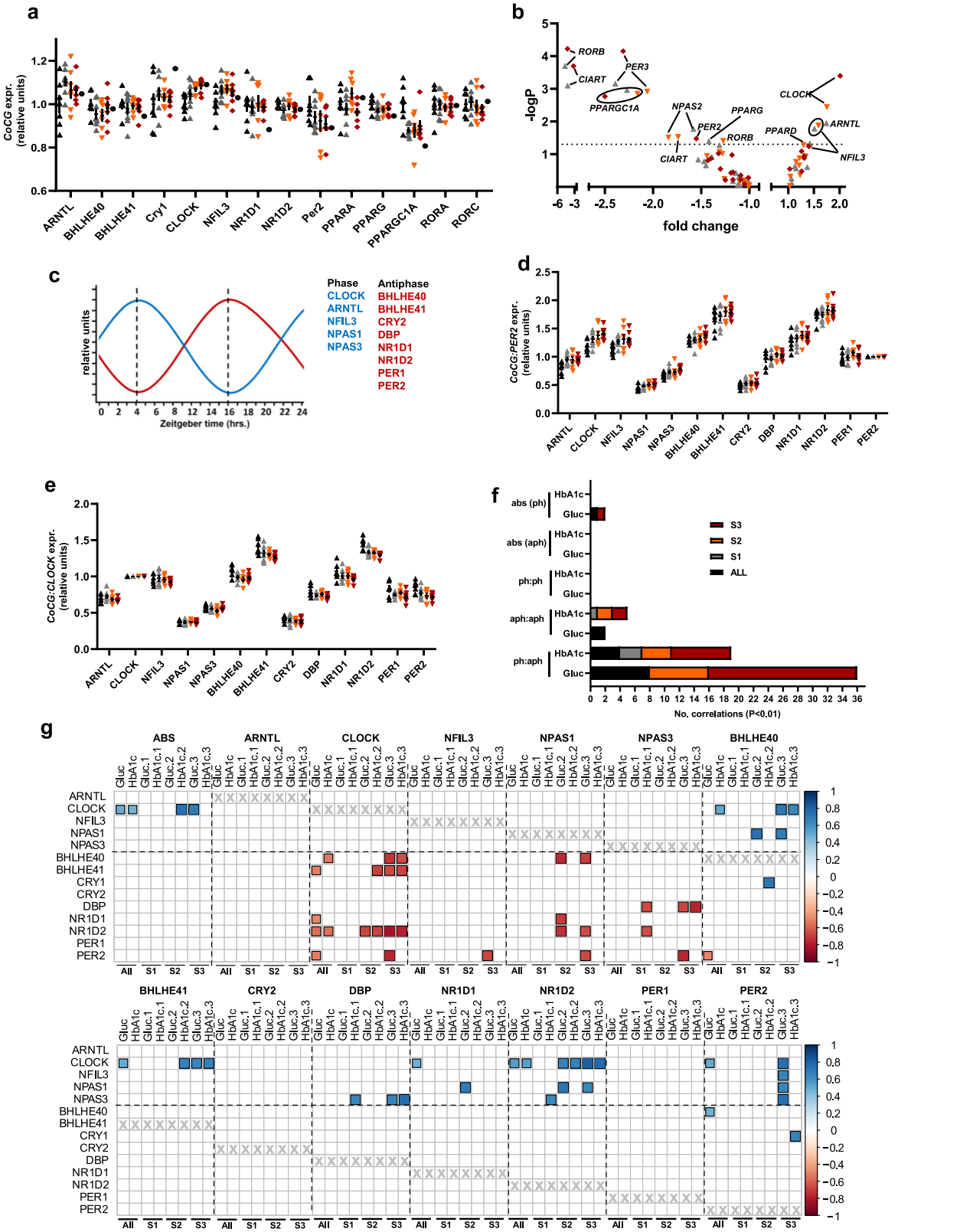

Fig. 4 | Increasing alterations of the circadian clock genes during the progression of T2D. a Gene expression of the main core-clock genes (*CoCGs*) on each group. **b** Differential expression of CoCGs known to be expressed in antiphase. **c** Representative plot of the phase and antiphase *CoCGs*. **d** Ratio of *CoCG:PER2* gene expression, and **e** *CoCG:CLOCK*. **f** Significant correlations ($P < 0.01$) for absolute (abs) values (ph or aph), or ratio between phase (ph) or antiphase (aph) *CoCG*, and glucose (Glu) or HbA1c. **g** Correlation heatmap from absolute (ABS) or ratio values of CoCGs, significant Spearman's correlation coefficients (rho) were colored blue (positive) and red (negative), ($P < 0.01$), NW ($n = 7$), OW ($n = 8$), PD ($n = 7$), T2D ($n = 8$), independent samples. Error bars as mean ± SEM.

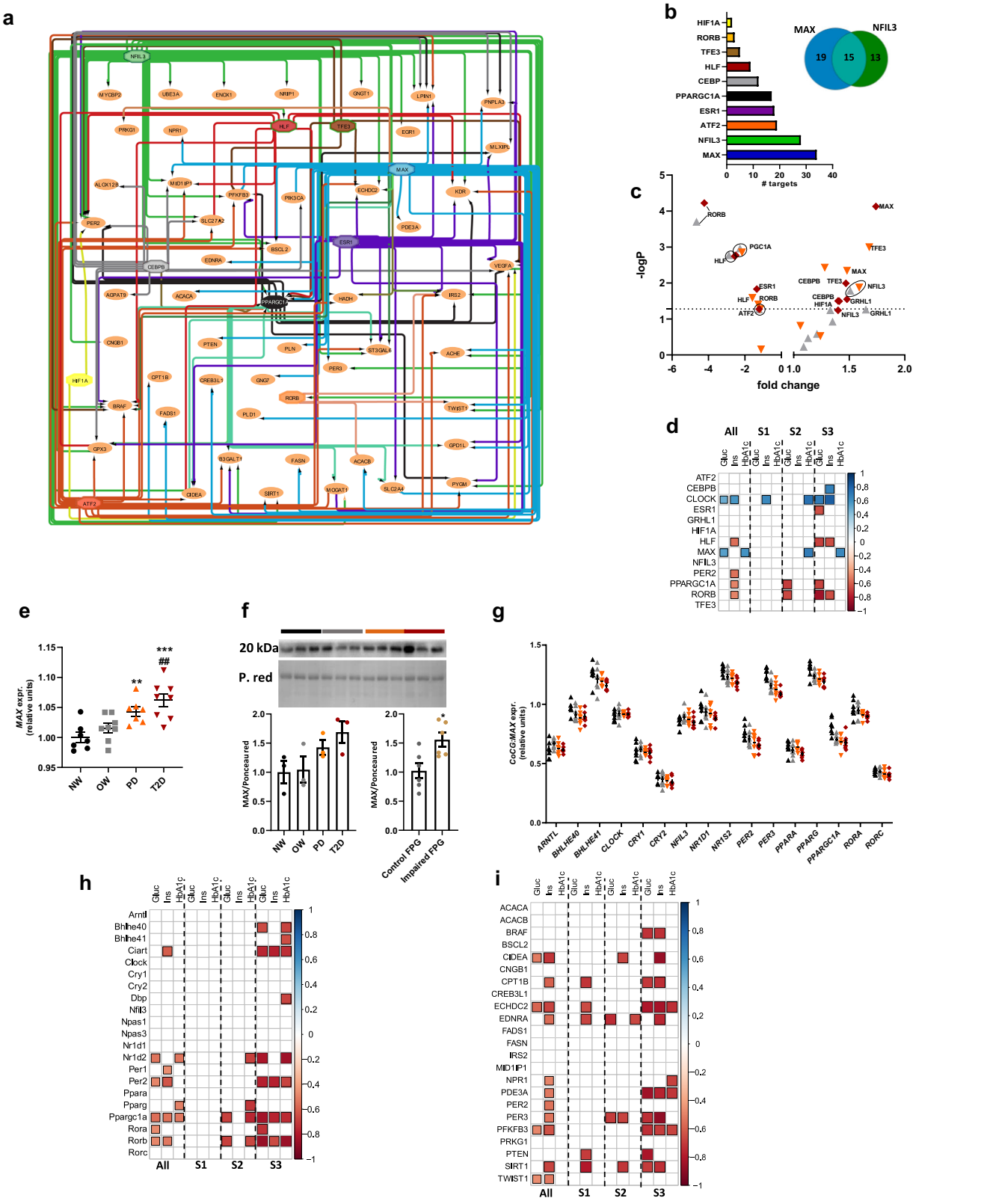

Circadian-expressed transcription factors involved in thermogenesis are dysregulated in T2D

Given the altered expression of CoCGs during the progression of the disease (Fig. 4) and the significant proportion of identified DEGs from the interactome being CCGs (Supplementary Fig. 4c, d), we aimed to identify potential transcription factors (TFs) modulating the expression of these genes. To this end, we conducted a promoter analysis on the interacting genes. Remarkably, *MAX* and *NFIL3* emerged as the TFs with the highest number of targets, followed by *ATF2, ESR1, PPARGC1A, CEBPB, HLF, TFE3, RORB*, and *HIF1A* (Fig. 5a–c). As these TFs potentially control genes involved in the catabolic process and thermogenesis, we analyzed the correlation between their expression and glucose metabolism parameters. In

Fig. 5 | Dysregulation of circadian-expressed transcription factors involved in thermogenesis and T2D. a Predicted transcription factors (TF) targeting interacting genes involved in thermogenesis and catabolism. **b** Bar graph of targets per TF, and Venn diagram depicting shared and exclusive targets for MAX and NFIL3. **c** Differential expression of TF per stage. **d** Correlation heatmap between gene expression and metabolism-related parameters (glucose, insulin, and HbA1c) per stage, significant Spearman's correlation coefficients (rho) were colored blue (positive) and red (negative), ($P < 0.01$). **e** *MAX* relative expression, ANOVA with eBayes, significant difference vs. NW group $^{**}P < 0.01$, $^{***}P < 0.001$, significant difference vs. OW group $^{\#\#}P < 0.01$. **f** MAX protein levels on SAT from NW (black), OW (gray), PD (orange), and T2D (red) individuals; MAX protein levels bar graph, one-way ANOVA followed by Tukey´s post-hoc test ($n = 3$). MAX protein levels on SAT from control (dark gray) and Impaired Fasting Plasma Glucose (FPG) (dark gold) individuals, t-test ($^{*}P < 0.05$) ($n = 6$). **g** Ratio of CoCG:MAX gene expression. Correlation heatmap between metabolism-related parameters (glucose, insulin, and HbA1c) **h** *CoCG:MAX* ratios, and **i** MAX target genes, per stage. Significant Spearman's correlation coefficients (rho) were colored blue (positive) and red (negative), $P < 0.01$. NW ($n = 7$), OW (n = 8), PD ($n = 7$), T2D ($n = 8$), independent samples. Error bars as mean ± SEM.

this context, an increasing association with metabolic parameters was observed during disease progression (Fig. 5d, Supplementary Fig. 11a). Notably, *PPARGC1A* showed a strong negative association in S2 and S3 (Supplementary Fig. 5, 11a, Supplementary Data 2).

While *MAX* and *NFIL3* exhibited about 50% overlap in their target genes (Fig. 5b), only *MAX* expression demonstrated a significant positive correlation with glucose metabolism parameters (Fig. 5d). Importantly, *MAX* showed a progressive increase in gene expression (Fig. 5e) and a tendency to increase in protein content in the T2D vs. NW groups (Fig. 5f). Since *MAX* is expressed in a circadian manner and has been recently identified as a CoCG[57,58], we calculated the ratio of gene expression between CoCGs and *MAX*. Interestingly, the ratio values gradually decreased, mirroring the patterns observed with *CLOCK* ratios (Figs. 4e, 5g). Moreover, correlation analysis revealed that the expression of some CoCGs in relation to *MAX* inversely correlate with clinical parameters linked to glucose metabolism (Fig. 5h). This supports the notion that MAX, is a core-clock repressor for BMAL-targeted genes, experiences both an increase and/or a phase-shift in its circadian repressive function during the progression of the disease[57,58].

Given that the predicted MAX targeted genes are crucial in the metabolic regulation of glucose and lipid metabolism and thermogenesis (Supplementary Fig. 11b), we analyzed the correlation between their expression values and clinical parameters related to glucose metabolism. Interestingly, most of these genes exhibited an increasingly inverse correlation with the clinical parameters (Fig. 5i, Supplementary Fig. 11c). These findings suggest that MAX plays a crucial role in the progressive circadian disruption of CoCGs and key CCGs involved in thermogenesis during the development of T2D.

Inflammatory processes are linked with the reduction of the thermogenic program during the progression of T2D

To explore the mechanisms underlying the altered expression of key TFs associated with the thermogenic program (Fig. 5a, b), we analyzed their promoters to identify regulatory factors involved in their transcriptional regulation. Interestingly, *IRF1, IRF3*, and *IRF8* emerged as key regulators of the expression of these TFs, with their expression levels increasing as the disease progressed (Fig. 6a–d).

Next, we constructed a protein-protein interactome network using these IRFs as "seeds", allowing the inclusion of additional interacting proteins (Fig. 6e). As expected, promoter analysis of the interacting genes confirmed the pivotal role of IRF1, IRF3, and IRF8 in regulating the expression of many of these genes (Fig. 6f). Moreover, virtually all the identified genes were upregulated (with only one downregulated at each stage), and all were DEGs at S3 (Fig. 6g).

Notably, enrichment analysis of the interactome revealed an increase in biological processes and pathways related to inflammation, including type I interferon signaling, positive regulation of the immune system, and inflammatory bowel disease. Diabetes-related pathways, such as insulin response, type I diabetes mellitus, and AGE-RAGE signaling in complications related to diabetes, were also identified (Fig. 6h). For instance, inflammation can impair sympathetic innervation by reducing Zn^{+} secretion from BAT and subcutaneous WAT, which involves the expression of several Zn^{+} transporters, including members of the solute carrier family 39 member (SLC39A1, SLC39A7) and metallothioneins (Mt1 and Mt2)[35]. Accordingly, we observed increased expression of genes from these families at S3, with a positive correlation with the metabolic parameters (Supplementary Fig. 12a–c).

Subsequently, we analyzed the correlation between the expression of the identified interactome genes and glucose metabolism-related clinical parameters. As expected, these genes showed a strong positive correlation with the clinical parameters, with the correlation strengthening as the disease progressed (Fig. 6I, Supplementary Fig. 13). These results not only confirm the contribution of inflammation to the progression of T2D[59], but also link inflammation to the inhibition of key processes involved in catabolic metabolism and the circadian clock through transcriptional responses.

Cellular integrity is compromised during the progression of T2D

Our findings support the notion that inflammation is linked to circadian and adipocyte dysfunction, as well as to a reduced thermogenic capacity (Figs. 2a–d, 3a–k, Supplementary Fig. 4b, 6a, b). To explore these mechanisms, we constructed a protein-protein interaction network using 13 selected genes involved in organelle homeostasis (*ATP2A3*, *BAK1*, *BAX*, *KEAP1*, *LRPPRC*, *NFE2L2*, *NLRC4*, *NLRP3*, *PLN*, *PPARGC1A*, *RYR1*, *SIRT1*, and *STIM1*) as "seed" genes, allowing the inclusion of additional interacting genes (Fig. 7a). The Gene Ontology (GO) analysis revealed biological processes associated with cellular integrity, including apoptosis, inflammasome, necroptosis, response to stress, response to UV, mitophagy, oxidative stress response, etc. (Fig. 7b). Notably, most of these genes exhibited an increasingly positive correlation with clinical parameters related to T2D (Fig. 7d).

About 60% and 81% of these DEGs were identified in S2 and S3, respectively, while 39% were found in S1. Interestingly, only 6% were unique to S1, compared to 12% and 25% in S2 and S3, highlighting the progressive nature of these cellular stress-related genes (Fig. 7c).

Interestingly cGMP signaling has been linked to tissue integrity[60,61] and with brown adipocyte activation[62]. For instance, Natriuretic peptide (NP) signaling, an upstream effector of the cGMP pathway, involves two key receptors: NPR1[63] which produces cGMP and NPR3, which degrades NP. Consequently, the *NPR1:NPR3 ratio* serves as a measure of brown adipocytes activation[64–66]. Our data revealed a consistent reduction in this ratio in the OWs groups (Fig. 7e). Which indicates an increase in organelle damage, as suggested by the identified processes including the BAK complex, BCL-2 family protein complex, and apoptosis (Fig. 7b). Specifically, *BAX* expression progressive increased through disease progression (Fig. 7f).

To further test this observation, we measured the protein levels of the pro-apoptotic proteins BAX and BAK. Consistently, both proteins were upregulated in the OW groups along with a higher level of their partner *PACS1* in these groups (Fig. 7g–i). Additionally, *NLRP3* was overexpressed in all the OW groups (Fig. 7j), acting as a cellular damage sensor that forms the inflammasome complex, which can precede apoptosis[67].

Our oxygen consumption experiments in differentiated beige adipocytes culture, showed that PD and T2D groups exhibited impaired respiratory capacity (Fig. 3b), a condition that triggers the mitochondrial-to-nucleus retrograde signaling (MTNRS) under stress and inflammation. This signaling reduces mitochondrial activity[68–71] and involves key mitochondrial regulators such as LRPPRC, SIRT1, and PPARGC1A[68–71]. In line with this, we found a reduced expression of *LRPPRC* and *PPARGC1A* in the OW

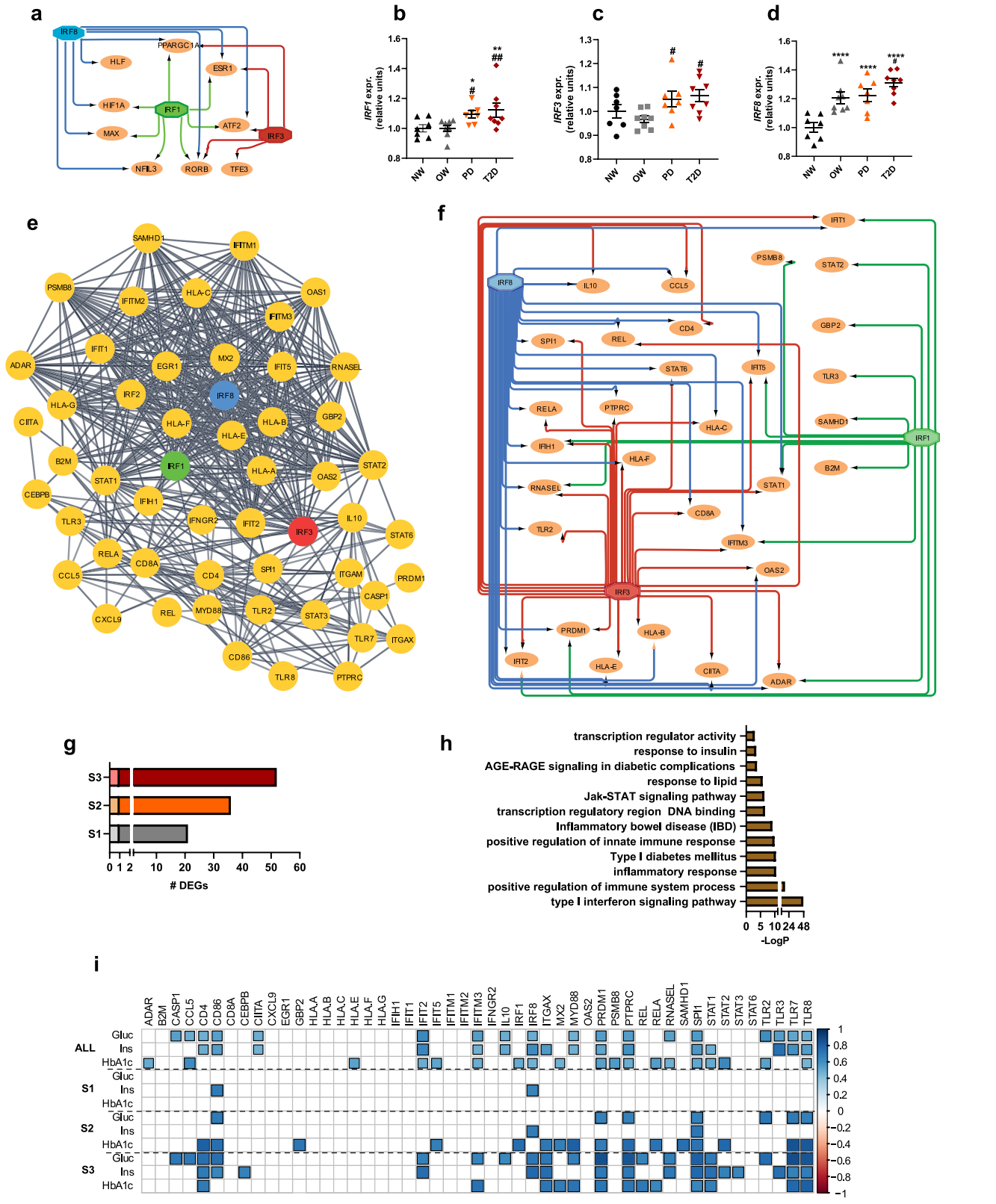

Fig. 6 | Inflammation is linked to an impairment in the thermogenic program during the progression of T2D. a Transcriptional network showing *IRF1, IRF3*, and *IRF8* as regulators of the identified TFs targeting thermogenic genes. **b-d** *IRF1, IRF3, and IRF8* relative expression, ANOVA with eBayes, significant difference vs. NW group $^{*}P < 0.05$, $^{**}P < 0.01$, $^{****}P < 0.0001$, significant difference vs. OW group $\#P < 0.05$, $\#\#P < 0.01$. **e** Protein-protein interactome network depicting known proteins interacting with IRF1, IRF3, and IRF8. **f** Transcriptional network from interacting proteins illustrating the role of IRF1, IRF3, and IRF8 in their regulation. **g** Interactome DEGs per stage. **h** Significantly enriched pathways from the interactome. **i** Correlation heatmap between metabolism-related parameters (glucose, insulin, and HbA1c) and interactome genes per stage. Significant Spearman's correlation coefficients (rho) were colored blue (positive) and red (negative), $P < 0.01$. NW ($n = 7$), OW ($n = 8$), PD ($n = 7$), T2D ($n = 8$), independent samples. Error bars as mean ± SEM.

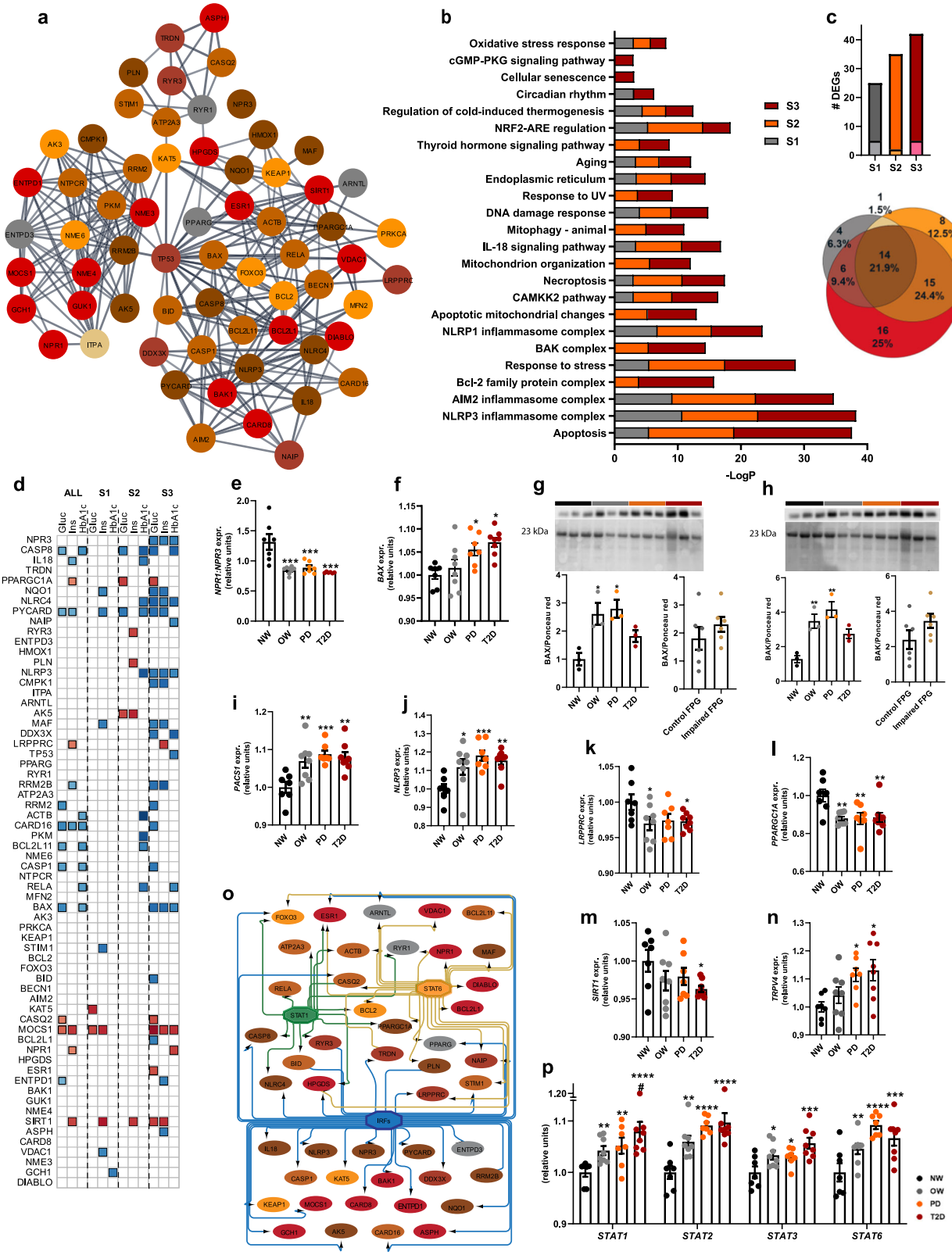

groups, and a significant decrease in *SIRT1* expression, specifically in the T2D group (Fig. 7k–m).

Strikingly, the Ca^{+2} channel TRPV4, a negative regulator of *PPARGC1A* expression in adipocytes, and a known contributor to inflammation and insulin resistance[72], showed a marked overexpression in a progressive manner (Fig. 7n), suggesting its involvement in the MTNRS. This overexpression is consistent with the observed mitochondrial dysfunction.

To identify potential transcriptional regulators of the stress-related proteins involved in these processes (Fig. 7a, b), we conducted promoter analyses. STAT1, STAT6, and several IRFs (IRF3, 4, 5, 7, 8, and 9) emerged as key transcription factors (TFs) involved in the regulation of these genes

Fig. 7 | Transcriptional response to organelle dysfunction during the progression of T2D. a Protein-protein interaction network of cellular stress-related genes is dysregulated during the progression of T2D. **b** Significantly enriched pathways from the interactome per stage. **c** Bar graph of DEGs, from the interactome per stage, and Venn diagram depicting shared and exclusive DEGs. **d** Correlation heatmap between metabolism-related parameters (glucose, insulin, and HbA1c) and interactome genes per stage, significant Spearman's correlation coefficients (rho) were colored blue (positive), $P < 0.01$. **e** *NPR1/NPR3* expression ratio. One-way ANOVA, followed by Tukey's post hoc test. Significant difference vs. NW group $^{***}P < 0.001$. **g** BAX and **h** BAK protein levels on SAT from NW, OW, PD, and T2D individuals. Bar graph protein levels on SAT from NW (black), OW (gray), PD (orange), and T2D (red) individuals, one-way ANOVA followed by Tukey´s post-hoc test ($n = 3$), $^{*}P < 0.05$, $^{**}P < 0.01$. Protein levels on SAT from control (dark gray) and Impaired Fasting Plasma Glucose (FPG) (dark gold) individuals, t-test ($n = 6$). **f** *BAX*, **i** *PACS1*, **j** *NLRP3*, **k** *LRPPRC*, **l** *PPARGC1A*, **m** *SIRT1*, **n** *TRPV4*, **p** *STAT1*, *STAT2*, *STAT3* relative expression, ANOVA with eBayes, significant difference vs. NW group $^{*}P < 0.05$, $^{**}P < 0.01$, $^{****}P < 0.0001$, significant difference vs. OW group #P < 0.05. **o** Transcriptional network of the interacting proteins. NW ($n = 7$), OW ($n = 8$), PD (n = 7), T2D ($n = 8$), independent samples. Error bars as mean ± SEM.

(Fig. 7o). Expression analysis further demonstrated a progressive increase in the levels of *STAT1, 2, 3*, and *6* (Fig. 7p). This family of TFs has been implicated in MTNRS, supporting the notion that mitochondrial dysfunction progressively precedes the development of T2D[73].

Finally, to gain insights into whether the identified processes are deregulated following obesity, we identified the DEGs by comparing the overweight groups as follows: S4 (OW vs PD), S5 (OW vs T2D), and S6 (PD vs T2D) from the interactomes (Supplementary Fig. 14a–c), which are involved in catabolism, inflammation, and cellular stress respectively. While we found a lower number of DEGs within the three comparison sets when comparing the stages S1-3, we observed a higher number of DEGs in the S6 from catabolism compared to the inflammation and cellular stress interactomes. This suggests that inflammation and cellular stress might precede metabolic regulatory processes during the development of T2D.

Discussion

Growing evidence suggest that brown and beige adipose tissues play a crucial role in regulating glucose and lipid metabolism, serving as metabolic sinks for these nutrients[6–10]. While animal models have supported the hypothesis that BAT/beige adipose tissues can ameliorate metabolic disorders and reduce blood glucose levels in patients with T2D[74]. Recently, clinical evidence has begun to corroborate this hypothesis in humans[8–10]. However, the cellular mechanisms by which brown/beige adipocytes function deteriorate during disease progression remain unclear.

By analyzing the SAT transcriptome of patients classified as normal weight (NW), overweight (OW), pre-diabetes (PD), and type 2 diabetes (T2D) (see Methods), we unveiled a progressive shift in its transcriptome that affects key processes related to transcriptional control, signaling pathways, and cellular functions. Importantly, pathways participating in the thermogenic program, such as cAMP, cGMP, and angiogenesis, were downregulated across all stages, with more pronounced suppression in later stages.

Interestingly, while S1 and S2 stages showed disruptions in thermogenic-related functions, like adrenergic receptor signaling, thyroid hormone signaling, and their downstream MAPK pathway, additional impairments were noted at S3. These included fatty acid β-oxidation, lipid catabolism, and positive regulation of cold-induced thermogenesis. This pattern suggests that the adipocytes' beiging capacity gradually deteriorates during the progression of T2D, likely due to the cumulative transcriptional alterations in key genes (Figs. 1a–f, 2a–d, Supplementary Fig. 4a, b). Indeed, we observed negative associations between glucose metabolism parameters and the expression of key genes involved in thermogenesis as well as essential metabolic sensors and regulators, such as *SIRT1, ERB3, PIK3CA, PPARGC1A, PTEN, CPT1B, CIDEA* among others[75–80], (Supplementary Fig. 5, 11c, Supplementary Data 2), reinforcing the link between impaired thermogenesis and worsening glucose metabolism in T2D.

Growing evidence highlights the importance of epigenetic modifications in the development of T2D[81,82]. For instance, ATAC-seq studies revealed differences in chromatin accessibility in specific loci between diabetic and non-diabetic pancreatic islet donors[83]. However, research on adipose tissues has predominantly focused on DNA methylation[81,82]. In our study, we observed an elevated expression of chromatin remodelers, such as *HDAC11* during the progression of T2D (Supplementary Fig. 3d–g). HDAC11 deficiency promotes thermogenesis and energy expenditure[23–26], suggesting a possible link between its upregulation and reduced thermogenic capacity in T2D.

Similarly, the histone H2A variant Y H2AY, (macroH2A1), is associated with regulating genes to lipid metabolism and adipocyte differentiation, in fact genetic ablation of this histone leads to increased leanness, improved glucose tolerance, and enhanced energy expenditure in mice fed with a high-fat diet[29]. Consistent with previous studies[30], we observed a progressive increase in *H2A.Y* expression from S1 to S3. Strikingly, H2AY acts as an epigenetic chromatin remodeler during the formation of senescence-associated heterochromatin foci-a complex process in which the chromatin regulator ASF1A plays a critical role[28]. Our data revealed an upregulation of *ASF1A* expression and other senescence-associated genes, including pro-inflammatory factors, interferon-regulated genes, (such as *CXCL1* and *NOX4*), (Supplementary Fig. 3h, i). Notably, cellular senescence is closely linked to T2D[27]. This highlights the importance of chromatin remodeling mechanisms in the development of T2D.

Another significant finding was the enrichment of circadian clock processes in all stages of the disease (Fig. 2a, d, Supplementary Fig. 4b). The expression of core-clock genes was also gradually altered during the progression of the disease (Fig. 4a–g, Supplementary Fig. 8a–m, 9, 10). In this regard, it has recently been observed that the number of WAT oscillatory genes is reduced in individuals with T2D compared with lean individuals[84].

The circadian clock orchestrates the expression of thousands of metabolic-related genes ensuring that these genes are expressed at the optimal time of the day to synchronize energy utilization and storage across the organism[48]. Its disruption has been strongly associated with the development of metabolic diseases and T2D[85–88]. In our study, we observed that the expression ratio values between pairs of core-clock genes, progressively diverge between groups and show strong correlations with clinical parameters (Fig. 4d–g, Supplementary Fig. 8a–m, 9, 10). This suggests that a gradual phase-shift and/or amplitude disruption in the oscillation of core-clock genes may play a significant role in the pathogenesis of T2D. Consequently, these circadian disruptions could serve as early markers for disease progression, reflecting a breakdown in the temporal coordination of metabolic processes.

This raises the question of how the circadian disruption in core-clock genes alters the expression of their downstream target genes. Our analysis of the promoter regions on DEGs coding for interacting proteins involved in thermogenesis and metabolism revealed the prominence of four major circadian-expressed transcription factors: NFIL3, MAX, PPARGC1A, and ATF2. Among these, *MAX* stood out as the only transcription factor that exhibited a progressive increase in expression (Fig. 5e, f), with a significant and consistent correlation with the onset and progression of T2D (Fig. 5d).

Remarkably, recent research has shown that MAX is indeed a core-clock gene, functioning as a transcriptional repressor for BMAL1 targets[57,58]. The progressive increase in *MAX* expression, particularly in the later stages of T2D, suggests that *MAX* may disrupt normal circadian feedback mechanisms, leading to two potential outcomes: (1) phase-shifting or altering the amplitude of circadian oscillations in core-clock genes and clock-controlled genes, and (2), repressing the expression of target genes, including both core-clock genes and metabolic effector genes. This hypothesis is supported by the lower core-clock gene:*MAX* ratios in

individuals with T2D, as well as the strong negative correlations between these ratios with several clinical parameters (Fig. 5g, h) and the progressive increase in the strength of the negative correlation between the expression of the predicted MAX target genes and the clinical parameters (Fig. 5i).

Our *in-silico* analysis revealed a link between MAX and inflammation, highlighting its potential roles as a transcriptional target of the interferon regulatory factors (IRFs) IRF1 and 8 (Fig. 6a–d). Indeed, *IRF3*, whose expression is higher in the T2D group (Fig. 6c), induces adipose tissue inflammation and reduces sympathetic tone and browning[89,90]. This provides a potential mechanism by which inflammation could contribute to thermogenic dysfunction in the context of T2D. Moreover, the non-coding RNA *mir193b-365* acts as a key inflammatory regulator by blocking the expression of MAX and reducing levels of *CCL2*, a pro-inflammatory factor in human adipocytes[91,92]. Interestingly, *mir193b-365* also plays a crucial role in brown fat differentiation[93], further reinforcing the role of MAX in thermogenic regulation and inflammation.

In this regard, the link between the circadian clock and inflammation has been demonstrated[94]. For example, in adipose tissue from obese patients, NFKB subunit NFKB1 and RELA block BMAL:CLOCK-mediated transcription, altering the expression of clock-controlled genes (CCGs). Inhibition of NFKB reduces metabolic inflammation and restores the expression of the core-clock gene *Per2* in mice[55]. Consistent with this, we observed a progressive induction of *RELA* along with a corresponding reduction in *PER2* and *PER3* (Figs. 4b, g, 6i, Supplementary Data 2). Therefore, the gradual increase in the inflammation during disease progression (Fig. 6a–i) may impair thermogenic program and insulin sensitivity[95,96], partly through circadian reprogramming of CCGs[97].

Although, we did not observe differences in the expression of the canonical thermogenic gene *UCP1*, other UCP1-independent mechanisms participate in energy dissipation, including futile cycles such as lipolysis/fatty acid re-esterification, creatine/phosphocreatine, SERCA-mediated calcium import and export cycles[98–101]. We found that obesity was associated with a decrease in the expression of genes involved in endoplasmic reticulum (ER) and sarcoplasmic reticulum (SR) calcium cycling, including *RYR1*, *RYR3*, *CASQ2*, and the key SERCA2b-regulatory protein phospholamban (*PLN*) (Supplementary Data 2). In skeletal muscle, PLN inhibits SERCA2b by reducing its calcium-binding affinity, forcing increased ATP consumption to transport calcium and thereby enhancing energy expenditure[100].

Moreover, in the absence of UCP1, beige adipocytes can function as a glucose sink, improving glucose tolerance independently of body weight via the norepinephrine-Adrb3-cAMP axis. This pathway induces the expression and activation of PLN, leading to an increase in intracellular Ca^{+2}, which further stimulates mitochondrial ATP synthesis at the expense of glucose as the primary fuel source. The resulting ATP is hydrolyzed by SERCA2b[102].

Intriguingly, some of the identified MAX targets are indeed involved in the cAMP and cGMP signaling pathways. On this regard, we identified NPR1 as a MAX target, which displays a reduced *NPR1*:*NPR3* ratio in all overweight conditions[64–66], supporting the notion that the alteration of different components of the cAMP and gGMP pathways reduces SNS-mediated browning during the progression of T2D[62,63]. This notion is further supported by the observed reduction in the protein level of TH[33,34].

Importantly, it has been observed that impaired mitochondrial respiratory capacity results in decreased expression on thermogenic and oxidative genes[8,9,102,103]. This is triggered by an increase in cytosolic Ca^{+2}, induced by mitochondrial oxidative stress, which activates the NLRP3 inflammasome pathway-dependent mitochondrial-to-nucleus retrograde signaling[71]. It also involves a down-regulation of the key mitochondrial regulator LRPPRC, which forms a transcriptional complex with PPARGC1A[68], and the key NAD+ dependent deacetylase SIRT1. SIRT1 deacetylates and activates PPARGC1A, thereby regulating the expression of mitochondrial genes and inducing mitochondrial activation[68,104–107].

Accordingly, we found that during the progression of T2D, *NLRP3* is gradually overexpressed while *LRPPR* and *PPARGC1A* were downregulated in all stages, and *SIRT1* at S3 (Fig. 7j–m). This implies that mitochondrial stress/dysfunction induces a transcriptional reprogramming of mitochondrial genes linked to the progression of T2D. Supporting this notion, we also found that the pro-apoptotic proteins BAX and BAK were upregulated at late stages. Moreover, PACS1, which contributes to the oligomerization of BAX and BAK and mitochondrial cell death[108] was upregulated in all stages (Fig. 7f–i). These proteins also participate in mitochondrial-to-nucleus retrograde communication, inducing the expression of proinflammatory genes under conditions of mitochondrial stress via STAT1-mediated activation of interferon-stimulated genes[109]. This is consistent with the increase of the TFs *STAT1-3* and *6* and *IRFs* (Figs. 6b–d, 7p).

Moreover, our data show that these proinflammatory transcription factors can be induced by the IRF1, 3, and 8 (Fig. 6f). Hence, during the progression of T2D, a mitochondrial-to-nucleus retrograde response induced by inflammatory mechanisms and cellular stress finally leads to a reduction in mitochondrial respiratory capacity, as reflected by the decrease in the BHI and SRC (Figs. 3e, f, k, 8a).

This implies that during the development of T2D, there is a reduction in the thermogenic capacity of SAT. This reduction is elicited by a complex vicious cycle involving several cellular and molecular mechanisms altered by environmental factors. First, various lifestyle habits, such as sleep/wake timing, feeding time, and a high-caloric diet, can disrupt the circadian clock. This can lead to weight gain and inflammation[54,110], exacerbating circadian misalignment and triggering transcriptional reprogramming, in part by key transcription factors such as IRFs, MAX, and STATs. Second, since MAX is a core-clock gene, this TF, along with inflammatory factors, may further reprogram the circadian transcriptome. This affects the temporal coordination of thousands of genes and proteins, disrupting cellular homeostasis. Third, these changes further impair mitochondrial function, which through mitochondrial retrograde pathways reprograms the expression of mitochondrial genes, reducing oxidative capacity (Fig. 8a, b). Prolonged exposure to this vicious cycle during aging, results in the progressive accumulation of transcriptionally altered genes, worsening cellular homeostasis and physiological condition[3].

Therefore, new chronotherapeutic approaches aimed at restoring the circadian clock or enhancing key regulators could interrupt this harmful cycle at one or several points, potentially preventing or even reversing the development of T2D[111].

Our study has certain limitations. While we conducted functional studies on cultured cells, most of our results were limited to transcriptional analysis with limited protein expressions and no post-translational modifications. Such modifications would more precisely reflect how these identified processes are being altered. In this context, proteomics and metabolomics experiments would be valuable for understanding how the identified transcriptional alterations affect cellular and biochemical processes during the progression of T2D. Additionally, chromatin immunoprecipitation experiments would be helpful for understanding the role of identified regulatory factors in the development of T2D.

Another limitation of our study is that samples were collected at a single time point in the circadian cycle. This limits our ability to analyze how different genes with varying acrophases might be affected at other times of day. To gain a more comprehensive understanding of circadian system alterations in each stage, sampling at multiple time points or analyzing synchronized beige cultures would be necessary. Additionally, the modest sample size, although representative, limits statistical power and subgroup analyses, such as exploring gender-specific effects. Larger cohorts would be necessary to confirm these findings and enhance the robustness of our conclusions. While obesity is a well-established risk factor for T2D, further exploration of the disease's progression in normal-weight individuals would provide valuable insights into mechanisms independent of adiposity.

Despite these limitations, to our knowledge, no previous study has examined the transcriptomic profile across the full spectrum of T2D in human adipose tissue. It highlights significant, stage-specific alterations in gene expression and offers a detailed view of the intricate changes that accompany T2D progression.

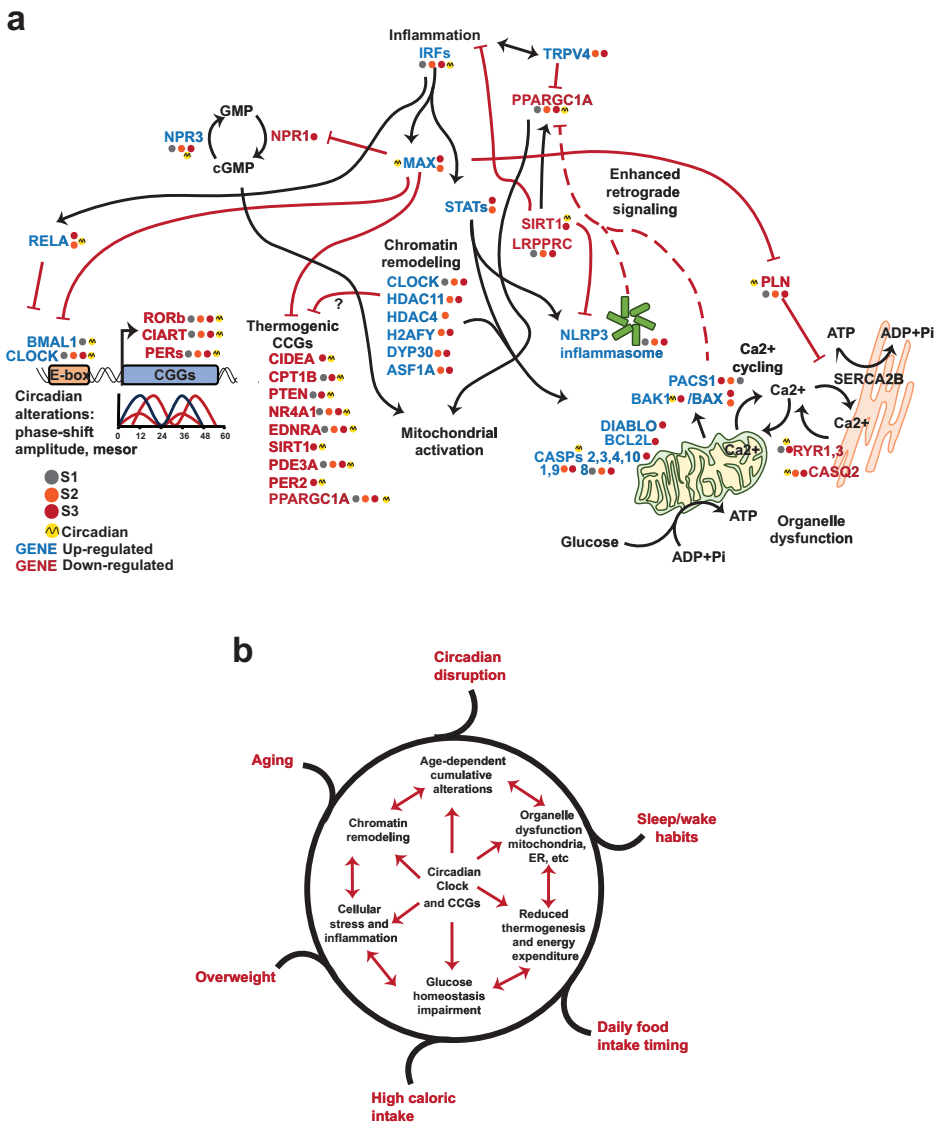

Fig. 8 | Progressive accumulation of transcriptional alterations during the progression of T2D reduces adipocyte thermogenic capacity. **a** Chronic inflammation under obese conditions, alters circadian gene expression through interferon-mediated responses of IRFs.In consequence, induces the expression of the NFKB p65 subunit RELA and the core clock transcription factor MAX at stages S2 and S3, disrupting the circadian translational transcriptional feedback loop (TTFL) mechanism[55,58] and affecting the expression of key CCGs. MAX, further exacerbates cellular dysfunction by repressing NPR1 and PLN, disrupting the pro-thermogenic cGMP signaling pathway[65,131] and impairing the Ca^{2+} cycling of the SERCA2-mediated futile cycle[102]. The Ca^{2+} channel TRPV4 inhibits the expression of PPARGC1A and induces inflammation[72], which, in turn, activates the STATs transcription factors, inducing NLRP3-inflammasome and pro-apoptotic genes, leading to a mitochondrial-to-nucleus retrograde signaling (MTNRS), contributing to reduced mitochondrial oxidative capacity[73,132]. In later stages, MAX may negatively regulate SIRT1-mediated activation of PPARGC1A[68,104–107] and the inhibition of the NLRP3-inflammasome[133,134]. Chromatin remodelers further regulate thermogenic and senescence-related genes[28,29]. **b** Environmental conditions induce a pro-inflammatory cascade, propelling a self-perpetuating vicious cycle that promotes cellular dysfunction, amplifies inflammation, and accumulates cellular and molecular defects, thereby exacerbating the progression of T2D.

In conclusion, our transcriptome analysis revealed a gradual accumulation of transcriptional alterations on SAT during T2D progression. Importantly, the dysregulation of the circadian clock from the early stage of the disease, might be critical on this alteration, in decrement of vital cellular processes regulating cellular metabolism and organelle function, favoring stress-induced responses such as inflammation, apoptosis, and mitochondrial dysfunction.

Methods

Human Subjects

Sixty-two females and twenty-six males (43.5 ± 23.5 years) were recruited. Sample sizes were not statistically predetermined but were in line with those used in other SAT transcriptome studies[112,113]. Men and women were divided into four groups according to their BMI, and the American Diabetes Association for prediabetes and diabetes criteria for fast glucose plasma (FGP) concentration and glycated hemoglobin (HbA1c) percentage[114]. Inclusion criteria: NW (BMI 18.5–24.9 kg/m^2), FPG 70–100 mg/dL and HbA1c < 5.7% (n = 22), OW (BMI 25–34.9 kg/m^2), FPG 70–100 mg/dL and HbA1c < 5.7%) (n = 23), PD (BMI 25–34.9 kg/m^2, FPG 110–125 mg/dL or OGTT ≥ 140 and < 200 mg/dL and HbA1c 5.7–6.4%) (n = 21), and T2D subjects (BMI 25–34.9 kg/m^2), FPG ≥ 126 mg/dL or OGTT ≥ 200 mg/dL, HbA1c ≥ 6.5%, with an initial diagnosis < 5 years and treated with metformin (n = 20). Exclusion criteria: Individuals who suffered from a 3rd and/or 4th degree burns at any time of life, catecholamine-secreting tumors, hyperthyroidism, and/or use of rosiglitazone.

Anthropometric measurements and body composition analysis

Anthropometric measurements were obtained under a 12-hour fasting condition by trained dietitians. Waist and hip circumferences were measured using a non-stretchable SECA 201 measuring tape with 0.1 cm precision. Height was measured with a SECA stadiometer, and weight was measured with a SECA mBCA 514 calibrated body composition analyzer. Body mass index (BMI) was calculated as weight (kg) divided by height (m^2). Body composition analysis was performed with dual-energy X-ray absorptiometry (DXA) (GE Healthcare, CoreScan software version).

Clinical and biochemical parameters

Systolic and diastolic blood pressure were measured by trained personnel while the participant was seated and at rest. Immediately following blood pressure measurement, venous blood samples were drawn by trained nurses. HbA1c plasma concentration was measured using high-performance liquid chromatography (HPLC) (variant II Turbo, BIORAD). Fasting insulin levels were determined by chemiluminescence immunoassay (Beckman Coulter Access 2). Plasma total cholesterol, triglycerides, and HDL-cholesterol were measured using colorimetric assays (Unicel DxC 600 Syncron Clinical System Beckman Coulter). LDL-cholesterol was calculated

using the Martin's equation. Plasma glucose concentration was measured with an automated glucose analyzer (Yellow Springs Instruments, OH, USA). Subcutaneous adipose tissue (SAT) biopsies and blood samples were taken between 7:00 and 8:00 h.

SAT biopsy and adipose-derived stem cell (ADSC) isolation

SAT biopsies were obtained by specialized surgeons in a sterile operating room. Local anesthesia was injected 3 cm below the umbilical area, and a small incision was made to collect the biopsy. Half was immediately frozen in liquid nitrogen and stored at -80°C. The remaining portion of the biopsy was used to isolate ADSCs. The tissue fragments were incubated with type I collagenase (Gibco™ 17101-015) diluted in 1x Hanks' Balanced Salt Solution (Gibco™ 14025-092) at a concentration of 0.025% for 60 min under constant shaking at 37°C. The cell suspension was centrifuged at 800 revolutions per minute (rpm) for 15 min. The pellet was resuspended in 3 mL of proliferation medium (High Glucose DMEM 1x (Gibco, 12100-046), 10% fetal bovine serum) (ByProducts, FBS19001), 1% Antibiotic-Antimycotic (Gibco, 15240-062), 1% MEM non-essential amino acids (Gibco, 11140-050), 1% GlutaMAX (Gibco, 35050061), and 1 mM Sodium Pyruvate (Gibco, 11360070). Cell suspension was filtered through a 100 µm pore cell strainer (Sigma Z742101-50EA) and centrifuged at 800 rpm for 15 min. The pellet was resuspended and seeded in a 60 cm^2 cell culture plate with proliferation medium. The dish was placed in an incubator at 37°C and 5% CO_2[115].

Cell culture and adipogenic differentiation

ADSCs were cultured in proliferation medium. Every 48 h, cells were washed with sterile PBS 1X, and proliferation medium was replaced until cells reached 100% confluence. ADSCs were used between passages 5 and 7.

For beige adipocyte differentiation, the cells were exposed to beige differentiation medium[116] which consisted of proliferation medium, 20 mM HEPES (Sigma, 12100-046), 1 µM insulin (PiSA, Insulex R), 1 µM rosiglitazone (Sigma, R2408), 1 µM Dexamethasone (Sigma, D1756), 500 µM IBMX (Sigma, I5879), 50 µM indomethacin (Sigma, I7378), 1 µM CL 316,243 disodium salt (Abcam, AB144605), and 250 nM 3,3´,5-triiodo-L-thyronine (Sigma, T2877). Every 48 h, cells were washed with sterile PBS 1X, and differentiation medium was replaced until ADSCs differentiation to beige adipocytes was completed within 15 days.

A small sample of ADSCs was differentiated to white adipocytes using the StemPro™ differentiation kit, following the manufacturer's instructions.

Oil red staining and quantification by spectrophotometry

Lipid droplet accumulation was visualized during the ADSCs differentiation for 21 days using the Oil-red-O staining technique. The differentiation medium was removed, and cells were fixed by washing them with PBS 1X. A 4% paraformaldehyde solution (Sigma 158127-500) was prepared by diluting with PBS 10X to a pH of 7.4, then added to the culture dish. After 30 min the fixing solution was removed.

The Oil Red O stock solution was prepared by dissolving 300 mg Oil-Red (Sigma, O0625) in 100 mL of 99% 2-propanol. The working solution was then made by diluting 24 mL of the stock solution with 16 mL of distilled water and was filtered through a Whatman (Sigma, WHA1004125) paper[117]. The cells were washed with distilled water, and 5 mL of oil red working solution was added, followed by incubation under constant, gentle shaking for 30 min at room temperature. Afterwards, the oil red working solution was removed, and the cells were rinsed three times with distilled water. They were then incubated with isoproterenol for 15 min on a plate shaker.

A 100 µL of the eluted oil red was used to measure the absorbance at 485 nm using a microplate reader (Synergy HTX Multi-Mode Reader) to determine lipid accumulation during the white and beige differentiation process[117].

Western blot

Forty milligrams of SAT were lysed in 200 µL of RIPA buffer (50 mM Tris–HCl pH 7.6, 150 mM NaCl, 1% NP-40, 0.5% sodium deoxycholate, and 0.1% SDS) supplemented with protease/phosphatase inhibitors (cOmplete Roche, PMSF 1 mM, Na3VO4 1 mM, and NaF 0.5 mM) using a TissueLyser LT (Qiagen) for two cycles of 2 min at 50 Hz. The samples were centrifuged for 15 min at 12,000 rpm at 4 °C. After removing the upper fat layer, the samples were centrifuged again for 15 min. Protein concentration was quantified using the Bradford method, and 20 µg of protein was loaded onto 10% or 12% polyacrylamide gels, resolved by SDS-PAGE, and transferred to 0.45 µm PVDF membranes (Immobilon, Merck). Membranes were blocked with 5% skim milk in TBS-Tween 0.05% and incubated overnight at 4 °C with gentle agitation in one of the following primary antibodies: mouse anti-Bak (AT38E2) 1:200 (SCBT sc-517390), mouse anti-Bax (B-9) 1:200 (SCBT sc-7480), rabbit anti-TH 1:1000 (Per Freez P40101), rabbit monoclonal anti-MAX 1:1000 (ab199489).

The secondary antibodies were HRP-conjugated anti-rabbit IgG (Cell Signaling 7074, 1:10,000) or HRP-conjugated anti-mouse IgG (Cell Signaling I8765, 1:10,000). HRP activity was detected with chemiluminescent substrate (Immobilon Western, Millipore WBKLS0500) in the Gel Logic 1500 imaging system (Kodak). Densitometric analysis was performed using the Gels function on the ImageJ software.

SAT RNA isolation

SAT biopsy RNA was isolated using the TRIzol method. A small sample was cut and incubated in 200 µL of TRIzol at room temperature for 5 min. The tissue was homogenized using an insulin syringe, and 40 µL of chloroform was added. The mixture was gently agitated manually and incubated at room temperature for 3 min. The samples were centrifuged at 12,000× *g* at 4 °C for 15 min. The upper aqueous phase was carefully transferred into a fresh tube. Following this, 100 µL of isopropanol and 0.5 µL of glycogen were added, and the mixture was incubated at room temperature for 10 min. The samples were centrifuged at 12,000× *g* at 4 °C for 10 min. Isopropanol was removed carefully. 200 µL of cold 70% ethanol was added, and the mixture was centrifuged at 17,000× *g* at 4 °C for 5 min. This step was repeated twice. Once the pellet was completely dried, it was resuspended in 15 µL of sterile distilled water. RNA was quantified using the Nanodrop 2000 (Thermo-Fisher Scientific™).

Mitochondrial DNA relative content analysis

Total DNA was isolated from differentiated adipocytes and SAT biopsies using the DNeasy Blood and Tissue Kit (Qiagen, 69504) following the manufacturer´s protocol. Quantification was performed by subjecting 10 ng of sonicated DNA to quantitative Real-Time PCR using iTaq Universal SYBR Green Supermix (Bio-Rad, 172-5121) analyzed with the QuantStudio™ Real-Time PCR Software. The ratio between the mitochondrial DNA-encoded gene cytochrome c oxidase subunit 1 (mtCOX1) and the nuclear gene 18S was calculated[118]. Primer concentration was 300 nM, and the sequences were as follows: mtCOX1 (Forward 5'-CCCACCGGCGT-CAAAGTATT-3', Reverse 5'-TTTGCTAATACAATGCCAGTCAGG-3'), and 18S (Forward 5'-ACAGGATTGACAGATTGATAGCTC-3', Reverse 5'-CAAATCGCTCCACCAACTAAGAA3').

Differentiated beige adipocytes oxygen consumption assay

Ten days prior to the assay, 5,000 cells were previously incubated for 5 days with the beige adipogenic differentiation medium and were then seeded on XFe96 culture plates (Agilent) treated with poly-L-lysine (Sigma P4832-50) overnight. The remaining differentiation process was carried out on XFe96 plates. The XF Cell Mito Stress Test Kit (Seahorse Bioscience, 103015-100) was used to perform the oxygen consumption assay, following the manufacturer's protocol.

On the day of the assay, differentiated beige adipocytes were washed with 200 µL of XF base medium without phenol red (103335-100), which contained 10 mM glucose, 1 mM sodium pyruvate, and 2 mM glutamine (pH adjusted to 7.4 at 37°C). Cells were incubated with 180 µL of the base medium in an incubator at 37°C without CO_2 for 1 h.

The previously hydrated cartridge was prepared with 200 µL of calibrating solution (Agilent) and inserted into the Seahorse XFe96

Analyzer™. Oxygen consumption rate was measured through the sequential inhibition of mitochondrial respiratory complexes. 1) Basal oxygen consumption; 2) inhibition of complex V by the injection of 2 µM oligomycin; 3) 1 µM of the mitochondrial uncoupler carbonyl cyanide p-trifluoromethoxyphenylhydrazone (FCCP); 4) inhibition of complex I and III with 1 µM of rotenone/antimycin; 5) 2-DG (2-deoxyglucose) was added at a concentration of 5 mM. The respiratory parameters were calculated with the following formulas[40,41,119]:

Non-mitochondrial respiration = (OCR rotenone/antimycin A)

Basal respiration = (OCR initial - Non-mitochondrial respiration)

ATP-linked respiration = (OCR initial – OCR oligomycin)

Maximal respiration = (OCR FCCP – Non-mitochondrial respiration)

Proton leak = (OCR oligomycin – Non-mitochondrial respiration)

Coupling efficiency = (Proton leak / ATP-linked respiration)

Spare respiratory capacity (SRC) = (Basal respiration / Maximal respiration)

Bioenergetic health index (BHI) = (SRC X ATP-linked respiration) / (Non-mitochondrial respiration X Proton leak)

Transcriptional profiling

Total RNA from approximately 20 mg of SAT tissue was extracted using 500 µL of TRIzol (Invitrogen) and quantified by UV spectroscopy (NanoDrop, Thermo Fisher Scientific). RNA quality was assessed with a RIN > 7.0 using the Bioanalyzer RNA 6000 (Agilent). Next, 150 ng of RNA was used for transcriptome analysis using the Clariom D Human microarray (Applied Biosystems) on a GeneChip 3000 scanner, performed by the INMEGEN Microarray Analysis Unit. Raw data was normalized, and gene expression values were obtained using the Transcriptome Analysis Console (TAC) 4.0 software (Thermo Fisher Scientific).

The analysis of Expression (Gene + Exon) with SST-RMA summarization method was employed to compare gene expression levels between groups S1 (NW vs. OW), S2 (NW vs. PD), and S3 (NW vs. T2D) using ANOVA with eBayes correction[120]. The differentially expressed coding genes among groups were identified based on the criteria of $P < 0.05$ and $|\log2(\text{Fold Change})| > 1.1$. The transcriptomic data are available at Gene Expression Omnibus GSE249298.

Bioinformatic analysis

Differentially expressed gene (DEG) sets between groups were visualized as volcano plots using GraphPad Prism 8.4 and as Venn diagrams using Venn Diagram Plotter 1.5.52. The sets were further analyzed for functional enrichment using Metascape, exploring the GO Biological Processes, Reactome Gene Sets, KEGG Pathway, and WikiPathways databases. Statistical significance was set at $P < 0.05$ (-logP >1.3). Therefore, a more positive (-log P) value indicates a lower probability that the observed enrichment is due to chance. The analysis considers the total gene library (N), the identified genes in each GO function (k), the gene list provided by the user (M), and the shared genes between k and M (n). The P values are calculated using the following formula[121].

$$p = \sum_{i=n}^{\min(M,K)} \binom{i}{n} \binom{N-k}{M-i}$$

Selected genes were analyzed to identify protein-protein interactions using the String plugin with a stringent cutoff score of 0.7[122]. Circadian clock-controlled genes (CCGs) were extracted from the "CircaDB" database, considering circadian oscillation using a JTK-P value of $P < 0.05$ for each gene[50]. The iRegulon plugin[123] on Cytoscape was employed to predict transcription factors driving the transcriptomic changes in selected genes, using the default parameters and the human database. Spearman correlation was used to identify correlations between the expression levels of selected genes and clinical parameters utilizing the 'Hmisc' and 'CorrPlot' packages for R[124]. A significant correlation was considered when $P < 0.05$.

Statistics and Reproducibility

Means ± standard error (SEM) were calculated, and different statistical tests were used. A t-test analysis was employed to compare two independent groups, a one-way ANOVA test followed by a post-hoc Tukey-Kramer test was applied to compare three or more independent groups, or Dunnet´s post-hoc when comparing a control group, provided that the variable data was normally distributed (Shapiro-Wilk $P > 0.05$) and homoscedastic (Bartlett's test $P > 0.05$). If the data did not meet the assumptions of ANOVA, the Kruskal-Wallis with Wilcoxon post-hoc test (non-normal and homoscedastic data) or Welch's ANOVA test with post-hoc Games-Howell test (for normal and heteroscedastic data) were used. The analyses were conducted using the 'moments', 'rstatix', and 'plotrix' packages for R[125–127]. Plots were obtained using GraphPad Prism 9.0. Factor analysis of mixed data (FAMD) was performed to analyze the association between quantitative (gene expression) and qualitative variables (diagnosis and sex). The FAMD was conducted using FactoMineR, and factoextra[128–130].

Reporting summary

Further information on research design is available in the Nature Portfolio Reporting Summary linked to this article.

Data availability

Data generated in this study are included in this published article and Supplementary Data 1. The data associated with this study are available from the corresponding author upon reasonable request. Transcriptomic data is available at Gene Expression Omnibus GSE249298.

Received: 8 May 2024; Accepted: 10 February 2025;
Published online: 08 March 2025

References

1. *World Health Organization: Diabetes fact sheets*, https://www.who.int/news-room/fact-sheets/detail/diabetes (2024).
2. Cho, N. H. et al. IDF Diabetes Atlas: Global estimates of diabetes prevalence for 2017 and projections for 2045. *Diab. Res. Clin. Pract.* **138**, 271–281 (2018).
3. Vázquez-Lizarraga, R. et al. Hypothalamic circuits and aging: keeping the circadian clock updated. *Neural Regenerat. Res.* 10.4103 (2024).
4. Guilherme, A., Henriques, F., Bedard, A. H. & Czech, M. P. Molecular pathways linking adipose innervation to insulin action in obesity and diabetes mellitus. *Nat. Rev. Endocrinol.* **15**, 207–225 (2019).
5. Villarroya, F., Cereijo, R., Villarroya, J. & Giralt, M. Brown adipose tissue as a secretory organ. *Nat. Rev. Endocrinol.* **13**, 26–35 (2017).
6. Chondronikola, M. et al. Brown Adipose Tissue Improves Whole-Body Glucose Homeostasis and Insulin Sensitivity in Humans. *Diabetes* **63**, 4089–4099 (2014).
7. Stanford, K. I. et al. Brown adipose tissue regulates glucose homeostasis and insulin sensitivity. *J. Clin. Investig.* **123**, 215–223 (2013).
8. Wibmer, A. G. et al. Brown adipose tissue is associated with healthier body fat distribution and metabolic benefits independent of regional adiposity. *Cell Rep. Med.* **2**, 100332 (2021).
9. Hibi, M. et al. Brown adipose tissue is involved in diet-induced thermogenesis and whole-body fat utilization in healthy humans. *Int J. Obes. (Lond.)* **40**, 1655–1661 (2016).
10. Becher, T. et al. Brown adipose tissue is associated with cardiometabolic health. *Nat. Med.* **27**, 58–65 (2021).
11. White, J. D., Dewal, R. S. & Stanford, K. I. The beneficial effects of brown adipose tissue transplantation. *Mol. Asp. Med* **68**, 74–81 (2019).
12. Shan, T. et al. Distinct populations of adipogenic and myogenic Myf5-lineage progenitors in white adipose tissues. *J. lipid Res.* **54**, 2214–2224 (2013).

13. Park, A., Kim, W. K. & Bae, K. H. Distinction of white, beige and brown adipocytes derived from mesenchymal stem cells. *World J. Stem Cells* **6**, 33–42 (2014).
14. Zuriaga, M. A., Fuster, J. J., Gokce, N. & Walsh, K. Humans and Mice Display Opposing Patterns of "Browning" Gene Expression in Visceral and Subcutaneous White Adipose Tissue Depots. *Front Cardiovasc Med* **4**, 27 (2017).
15. Giordano, A., Frontini, A. & Cinti, S. Convertible visceral fat as a therapeutic target to curb obesity. *Nat. Rev. Drug Discov.* **15**, 405–424 (2016).
16. Kaisanlahti, A. & Glumoff, T. Browning of white fat: agents and implications for beige adipose tissue to type 2 diabetes. *J. Physiol. Biochem.* **75**, 1–10 (2019).
17. Harms, M. J. et al. Mature human white adipocytes cultured under membranes maintain identity, function, and can transdifferentiate into brown-like adipocytes. *Cell Rep.* **27**, 213–225.e215 (2019).
18. Cypess, A. M. et al. Activation of human brown adipose tissue by a beta3-adrenergic receptor agonist. *Cell Metab.* **21**, 33–38 (2015).
19. Li, T. et al. Type 2 diabetes is more predictable in women than men by multiple anthropometric and biochemical measures. *Sci. Rep.* **11**, 6062 (2021).
20. Kautzky-Willer, A., Leutner, M. & Harreiter, J. Sex differences in type 2 diabetes. *Diabetologia* **66**, 986–1002 (2023).
21. Petrus, P. et al. Adipocyte Expression of SLC19A1 Links DNA Hypermethylation to Adipose Tissue Inflammation and Insulin Resistance. *J. Clin. Endocrinol. Metab.* **103**, 710–721 (2018).
22. Glass, C. K. & Olefsky, J. M. Inflammation and lipid signaling in the etiology of insulin resistance. *Cell Metab.* **15**, 635–645 (2012).
23. Bagchi, R. A. *et al*. HDAC11 suppresses the thermogenic program of adipose tissue via BRD2. *JCI insight* **3** https://doi.org/10.1172/jci.insight.120159 (2018).
24. Yang, H. et al. HDAC11 deficiency resists obesity by converting adipose-derived stem cells into brown adipocyte-like cells. *Int. J. Biol. Macromol.***258**, 128852 (2024).
25. Sun, L. et al. Programming and Regulation of Metabolic Homeostasis by HDAC11. *eBioMedicine* **33**, 157–168 (2018).
26. Chen, H., Xie, C., Chen, Q. & Zhuang, S. HDAC11, an emerging therapeutic target for metabolic disorders. *Front Endocrinol. (Lausanne)* **13**, 989305 (2022).
27. Smith, U., Li, Q., Rydén, M. & Spalding, K. L. Cellular senescence and its role in white adipose tissue. *Int. J. Obes.* **45**, 934–943 (2021).
28. Zhang, R. et al. Formation of MacroH2A-Containing Senescence-Associated Heterochromatin Foci and Senescence Driven by ASF1a and HIRA. *Dev. Cell* **8**, 19–30 (2005).
29. Sheedfar, F. et al. Genetic ablation of macrohistone H2A1 leads to increased leanness, glucose tolerance and energy expenditure in mice fed a high-fat diet. *Int. J. Obes.* **39**, 331–338 (2015).
30. Pazienza, V. et al. Histone macroH2A1.2 promotes metabolic health and leanness by inhibiting adipogenesis. *Epigenet. Chromatin* **9**, 45 (2016).
31. Cheng, Y. et al. Prediction of Adipose Browning Capacity by Systematic Integration of Transcriptional Profiles. *Cell Rep.* **23**, 3112–3125 (2018).
32. Perdikari, A. et al. BATLAS: Deconvoluting Brown Adipose Tissue. *Cell Rep.* **25**, 784–797.e784 (2018).
33. Ruan, H. B. et al. O-GlcNAc Transferase Enables AgRP Neurons to Suppress Browning of White Fat. *Cell* **159**, 306–317 (2014).
34. Yang, X. & Ruan, H.-B. Neuronal Control of Adaptive Thermogenesis. *Front. Endocrinol.* **6** https://doi.org/10.3389/fendo.2015.00149 (2015).
35. Jiang, J. et al. Thermogenic adipocyte-derived zinc promotes sympathetic innervation in male mice. *Nat. Metab.* **5**, 481–494 (2023).
36. Murphy, M. P. & Hartley, R. C. Mitochondria as a therapeutic target for common pathologies. *Nat. Rev. Drug Discov.* **17**, 865–886 (2018).
37. Heinonen, S. et al. Impaired mitochondrial biogenesis in adipose tissue in acquired obesity. *Diabetes* **64**, 3135–3145 (2015).
38. Pisani, D. F. et al. Mitochondrial fission is associated with UCP1 activity in human brite/beige adipocytes. *Mol. Metab.* **7**, 35–44 (2018).
39. Donnell, R. A., Carré, J. E. & Affourtit, C. Acute bioenergetic insulin sensitivity of skeletal muscle cells: ATP-demand-provoked glycolysis contributes to stimulation of ATP supply. *Biochem. Biophys. Rep.* **30**, 101274 (2022).
40. Pfleger, J., He, M. & Abdellatif, M. Mitochondrial complex II is a source of the reserve respiratory capacity that is regulated by metabolic sensors and promotes cell survival. *Cell Death Dis.* **6**, e1835–e1835 (2015).
41. Chacko, B. K. et al. The Bioenergetic Health Index: a new concept in mitochondrial translational research. *Clin. Sci.* **127**, 367–373 (2014).
42. Fleckenstein-Elsen, M. et al. Eicosapentaenoic acid and arachidonic acid differentially regulate adipogenesis, acquisition of a brite phenotype and mitochondrial function in primary human adipocytes. *Mol. Nutr. Food Res* **60**, 2065–2075 (2016).
43. Bohm, A. et al. Increased mitochondrial respiration of adipocytes from metabolically unhealthy obese compared to healthy obese individuals. *Sci. Rep.* **10**, 12407 (2020).
44. Czajka, A. et al. Altered Mitochondrial Function, Mitochondrial DNA and Reduced Metabolic Flexibility in Patients With Diabetic Nephropathy. *EBioMedicine* **2**, 499–512 (2015).
45. Calton, E. K., Keane, K. N., Soares, M. J., Rowlands, J. & Newsholme, P. Prevailing vitamin D status influences mitochondrial and glycolytic bioenergetics in peripheral blood mononuclear cells obtained from adults. *Redox Biol.* **10**, 243–250 (2016).
46. Pizarro, A., Hayer, K., Lahens, N. F. & Hogenesch, J. B. CircaDB: a database of mammalian circadian gene expression profiles. *Nucleic acids Res.* **41**, D1009–D1013 (2012).
47. Ruben, M. D. et al. A database of tissue-specific rhythmically expressed human genes has potential applications in circadian medicine. *Sci. Transl. Med.* **10**, eaat8806 (2018).
48. Koronowski, K. B. & Sassone-Corsi, P. Communicating clocks shape circadian homeostasis. *Science* **371**, eabd0951 (2021).
49. Rizza, S. et al. Alterations in Rev-ERBα/BMAL1 ratio and glycated hemoglobin in rotating shift workers: The EuRhythDia study. *Acta Diabetologica* **58**, 1111–1117 (2021).
50. Pizarro, A., Hayer, K., Lahens, N. F. & Hogenesch, J. B. CircaDB: a database of mammalian circadian gene expression profiles. *Nucleic acids Res.* **41**, D1009–D1013 (2013).
51. Buxton, O. M. et al. Adverse metabolic consequences in humans of prolonged sleep restriction combined with circadian disruption. *Sci. Transl. Med.* **4**, 129ra143 (2012).
52. Morris, C. J. et al. Endogenous circadian system and circadian misalignment impact glucose tolerance via separate mechanisms in humans. *Proc. Natl. Acad. Sci. USA* **112**, E2225–E2234 (2015).
53. Gabriel, B. M. et al. Disrupted circadian oscillations in type 2 diabetes are linked to altered rhythmic mitochondrial metabolism in skeletal muscle. *Sci. Adv.* **7**, eabi9654 (2021).
54. Eckel-Mahan, K. L. et al. Reprogramming of the circadian clock by nutritional challenge. *Cell* **155**, 1464–1478 (2013).
55. Maury, E., Navez, B. & Brichard, S. M. Circadian clock dysfunction in human omental fat links obesity to metabolic inflammation. *Nat. Commun.* **12**, 2388 (2021).
56. Kalsbeek, A., la Fleur, S. & Fliers, E. Circadian control of glucose metabolism. *Mol. Metab.* **3**, 372–383 (2014).
57. Burchett, J. B., Knudsen-Clark, A. M. & Altman, B. J. MYC ran up the clock: The complex interplay between MYC and the molecular circadian clock in cancer. *Int. J. Mol. Sci.* **22**, 7761 (2021).

58. Blaževitš, O. et al. MYC-associated factor MAX is a regulator of the circadian clock. *Int. J. Mol. Sci.* **21**, 2294 (2020).
59. SantaCruz-Calvo, S. et al. Adaptive immune cells shape obesity-associated type 2 diabetes mellitus and less prominent comorbidities. *Nat. Rev. Endocrinol.* **18**, 23–42 (2022).
60. Rappaport, J. A. & Waldman, S. A. The Guanylate Cyclase C—cGMP Signaling Axis Opposes Intestinal Epithelial Injury and Neoplasia. *Front. Oncol.* **8** https://doi.org/10.3389/fonc.2018.00299 (2018).
61. Lehners, M., Dobrowinski, H., Feil, S. & Feil, R. cGMP Signaling and Vascular Smooth Muscle Cell Plasticity. *J Cardiovasc Dev Dis* **5** https://doi.org/10.3390/jcdd5020020 (2018).
62. Mitschke, M. M. et al. Increased cGMP promotes healthy expansion and browning of white adipose tissue. *FASEB J.* **27**, 1621–1630 (2013).
63. Bordicchia, M. et al. Cardiac natriuretic peptides act via p38 MAPK to induce the brown fat thermogenic program in mouse and human adipocytes. *J. Clin. Invest* **122**, 1022–1036 (2012).
64. Wu, J., Cohen, P. & Spiegelman, B. M. Adaptive thermogenesis in adipocytes: Is beige the new brown? *Genes Dev.* **27**, 234–250 (2013).
65. Kovacova, Z. et al. Adipose tissue natriuretic peptide receptor expression is related to insulin sensitivity in obesity and diabetes. *Obesity* **24**, 820–828 (2016).
66. Bae, I.-S. & Kim, S. H. Expression and secretion of an atrial natriuretic peptide in beige-like 3T3-L1 adipocytes. *Int. J. Mol. Sci.* **20**, 6128 (2019).
67. Huang, Y., Xu, W. & Zhou, R. NLRP3 inflammasome activation and cell death. *Cell. Mol. Immunol.* **18**, 2114–2127 (2021).
68. Nam, M. et al. Mitochondrial retrograde signaling connects respiratory capacity to thermogenic gene expression. *Sci. Rep.* **7**, 2013 (2017).
69. Burgener, A.-V. et al. SDHA gain-of-function engages inflammatory mitochondrial retrograde signaling via KEAP1–Nrf2. *Nat. Immunol.* **20**, 1311–1321 (2019).
70. Vizioli, M. G. et al. Mitochondria-to-nucleus retrograde signaling drives formation of cytoplasmic chromatin and inflammation in senescence. *Genes Dev.* **34**, 428–445 (2020).
71. Arruda, A. P. & Hotamisligil, G. S. Calcium homeostasis and organelle function in the pathogenesis of obesity and diabetes. *Cell Metab.* **22**, 381–397 (2015).
72. Ye, L. et al. TRPV4 Is a Regulator of Adipose Oxidative Metabolism, Inflammation, and Energy Homeostasis. *Cell* **151**, 96–110 (2012).
73. Meier, J. A. et al. Stress-induced dynamic regulation of mitochondrial STAT3 and its association with cyclophilin D reduce mitochondrial ROS production. *Sci. Signal.* **10**, eaag2588 (2017).
74. Lapa, C. et al. Whitening and impaired glucose utilization of brown adipose tissue in a rat model of type 2 diabetes mellitus. *Sci. Rep.* **7**, 16795 (2017).
75. Nelson, V. L., Jiang, Y. P., Dickman, K. G., Ballou, L. M. & Lin, R. Z. Adipose tissue insulin resistance due to loss of PI3K p110α leads to decreased energy expenditure and obesity. *Am. J. Physiol. Endocrinol. Metab.* **306**, E1205–E1216 (2014).
76. Ma, Y., Gao, M. & Liu, D. Preventing high fat diet-induced obesity and improving insulin sensitivity through neuregulin 4 gene transfer. *Sci. Rep.* **6**, 26242 (2016).
77. Puigserver, P. et al. A Cold-Inducible Coactivator of Nuclear Receptors Linked to Adaptive Thermogenesis. *Cell* **92**, 829–839 (1998).
78. Ortega-Molina, A. et al. Pten Positively Regulates Brown Adipose Function, Energy Expenditure, and Longevity. *Cell Metab.* **15**, 382–394 (2012).
79. Patel, B. V. et al. Emergent Coordination of the CHKB and CPT1B Genes in Eutherian Mammals: Implications for the Origin of Brown Adipose Tissue. *J. Mol. Biol.* **432**, 6127–6145 (2020).
80. Molina-Ayala, M. A. et al. Expression of obesity-and type-2 diabetes-associated genes in omental adipose tissue of individuals with obesity. *Gene* **815**, 146181 (2022).
81. Ling, C. & Rönn, T. Epigenetics in Human Obesity and Type 2 Diabetes. *Cell Metab.* **29**, 1028–1044 (2019).
82. Ling, C., Bacos, K. & Rönn, T. Epigenetics of type 2 diabetes mellitus and weight change — a tool for precision medicine? *Nat. Rev. Endocrinol.* **18**, 433–448 (2022).
83. Volkov, P. et al. Whole-genome bisulfite sequencing of human pancreatic islets reveals novel differentially methylated regions in type 2 diabetes pathogenesis. *Diabetes* **66**, 1074–1085 (2017).
84. Stenvers, D. J. et al. Diurnal rhythms in the white adipose tissue transcriptome are disturbed in obese individuals with type 2 diabetes compared with lean control individuals. *Diabetologia* **62**, 704–716 (2019).
85. Vetter, C. et al. Night shift work, genetic risk, and type 2 diabetes in the UK biobank. *Diab. care* **41**, 762–769 (2018).
86. Minchenko, D. O. Expression of circadian genes in subcutaneous adipose tissue of obese men with glucose intolerance and Type 2 diabetes. *J. Exp. Integrat. Med.* **5** (2015).
87. Ando, H. et al. Clock gene expression in the liver and adipose tissues of non-obese type 2 diabetic Goto-Kakizaki rats. *Clin. Exp. Hypertension* **31**, 201–207 (2009).
88. Otway, D. T. et al. Rhythmic Diurnal Gene Expression in Human Adipose Tissue From Individuals Who Are Lean, Overweight, and Type 2 Diabetic. *Diabetes* **60**, 1577–1581 (2011).
89. Kumari, M. et al. IRF3 promotes adipose inflammation and insulin resistance and represses browning. *J. Clin. Investig.* **126**, 2839–2854 (2016).
90. Sindhu, S. et al. Increased adipose tissue expression of interferon regulatory factor (IRF)-5 in obesity: association with metabolic inflammation. *Cells* **8**, 1418 (2019).
91. Kulyté, A. et al. Additive effects of microRNAs and transcription factors on CCL2 production in human white adipose tissue. *Diabetes* **63**, 1248–1258 (2014).
92. Arner, E. et al. Adipose tissue microRNAs as regulators of CCL2 production in human obesity. *Diabetes* **61**, 1986–1993 (2012).
93. Sun, L. et al. Mir193b–365 is essential for brown fat differentiation. *Nat. cell Biol.* **13**, 958–965 (2011).
94. Orozco-Solis, R. & Aguilar-Arnal, L. Circadian Regulation of Immunity Through Epigenetic Mechanisms. *Front. Cell. Infecti. Microbiol.* **10** https://doi.org/10.3389/fcimb.2020.00096 (2020).
95. van den Berg, S. M., van Dam, A. D., Rensen, P. C., de Winther, M. P. & Lutgens, E. Immune modulation of brown (ing) adipose tissue in obesity. *Endocr. Rev.* **38**, 46–68 (2017).
96. Pirzgalska, R. M. et al. Sympathetic neuron–associated macrophages contribute to obesity by importing and metabolizing norepinephrine. *Nat. Med.* **23**, 1309–1318 (2017).
97. Froy, O. & Garaulet, M. The Circadian Clock in White and Brown Adipose Tissue: Mechanistic, Endocrine, and Clinical Aspects. *Endocr. Rev.* **39**, 261–273 (2018).
98. Liu, X., Rossmeisl, M., McClaine, J. & Kozak, L. P. Paradoxical resistance to diet-induced obesity in UCP1-deficient mice. *J. Clin. Investig.* **111**, 399–407 (2003).
99. Chouchani, E. T., Kazak, L. & Spiegelman, B. M. New advances in adaptive thermogenesis: UCP1 and beyond. *Cell Metab.* **29**, 27–37 (2019).
100. Brownstein, A. J., Veliova, M., Acin-Perez, R., Liesa, M. & Shirihai, O. S. ATP-consuming futile cycles as energy dissipating mechanisms to counteract obesity. *Rev. Endocr. Metab. Disord.* **23**, 121–131 (2022).
101. Rahbani, J. F. et al. Creatine kinase B controls futile creatine cycling in thermogenic fat. *Nature* **590**, 480–485 (2021).

102. Ikeda, K, et al. UCP1-independent signaling involving SERCA2b-mediated calcium cycling regulates beige fat thermogenesis and systemic glucose homeostasis. *Nat. Med.* **23**, 1454 (2017).
103. Park, E.-J. et al. Ssu72 phosphatase is essential for thermogenic adaptation by regulating cytosolic translation. *Nat. Commun.* **14**, 1097 (2023).
104. Price, N. L. et al. SIRT1 is required for AMPK activation and the beneficial effects of resveratrol on mitochondrial function. *Cell Metab.* **15**, 675–690 (2012).
105. Lagouge, M. et al. Resveratrol improves mitochondrial function and protects against metabolic disease by activating SIRT1 and PGC-1α. *Cell* **127**, 1109–1122 (2006).
106. Rodgers, J. T. et al. Nutrient control of glucose homeostasis through a complex of PGC-1α and SIRT1. *Nature* **434**, 113–118 (2005).
107. Vellinga, T. T. et al. SIRT1/PGC1α-dependent increase in oxidative phosphorylation supports chemotherapy resistance of colon cancer. *Clin. cancer Res.* **21**, 2870–2879 (2015).
108. Brasacchio, D. et al. Epigenetic control of mitochondrial cell death through PACS1-mediated regulation of BAX/BAK oligomerization. *Cell Death Differ.* **24**, 961–970 (2017).
109. Tigano, M., Vargas, D. C., Tremblay-Belzile, S., Fu, Y. & Sfeir, A. Nuclear sensing of breaks in mitochondrial DNA enhances immune surveillance. *Nature* **591**, 477–481 (2021).
110. Hatori, M. et al. Time-restricted feeding without reducing caloric intake prevents metabolic diseases in mice fed a high-fat diet. *Cell Metab.* **15**, 848–860 (2012).
111. Escalante-Covarrubias, Q. et al. Time-of-day defines NAD+ efficacy to treat diet-induced metabolic disease by synchronizing the hepatic clock in mice. *Nat. Commun.* **14**, 1685 (2023).
112. Rey, F. et al. Transcriptome Analysis of Subcutaneous Adipose Tissue from Severely Obese Patients Highlights Deregulation Profiles in Coding and Non-Coding Oncogenes. *Int. J. Mol. Sci.* **22**, 1989 (2021).
113. Berardo, C. et al. Subcutaneous Adipose Tissue Transcriptome Highlights Specific Expression Profiles in Severe Pediatric Obesity: A Pilot Study. *Cells* **12**, 1105 (2023).
114. ElSayed, N. A. et al. 2. Classification and Diagnosis of Diabetes: Standards of Care in Diabetes—2023. *Diab. Care* **46**, S19–S40 (2022).
115. Ge, X. et al. Isolation and culture of human adipose-derived stem cells from subcutaneous and visceral white adipose tissue compartments. *Bio-Protoc.* **6**, e2027–e2027 (2016).
116. Blumenfeld, N. R. et al. A direct tissue-grafting approach to increasing endogenous brown fat. *Sci. Rep.* **8**, 7957 (2018).
117. Kraus, N. A. et al. Quantitative assessment of adipocyte differentiation in cell culture. *Adipocyte* **5**, 351–358 (2016).
118. Bell, E. L. et al. The Qo site of the mitochondrial complex III is required for the transduction of hypoxic signaling via reactive oxygen species production. *J. Cell Biol.* **177**, 1029–1036 (2007).
119. Schmidt, C. A., Fisher-Wellman, K. H. & Neufer, P. D. From OCR and ECAR to energy: Perspectives on the design and interpretation of bioenergetics studies. *J. Biol. Chem.* **297**, 101140 (2021).
120. Ritchie, M. E. et al. limma powers differential expression analyses for RNA-sequencing and microarray studies. *Nucleic acids Res.* **43**, e47 (2015).
121. Zhou, Y. et al. Metascape provides a biologist-oriented resource for the analysis of systems-level datasets. *Nat. Commun.* **10**, 1523 (2019).
122. Szklarczyk, D. et al. The STRING database in 2021: customizable protein-protein networks, and functional characterization of user-uploaded gene/measurement sets. *Nucleic acids Res.* **49**, D605–d612 (2021).
123. Janky, R. et al. iRegulon: From a Gene List to a Gene Regulatory Network Using Large Motif and Track Collections. *PLOS Computat. Biol.* **10**, e1003731 (2014).
124. Wei, T. et al. Package 'corrplot'. *Statistician* **56**, e24 (2017).
125. Komsta, L. & Novomestky, F. Moments, cumulants, skewness, kurtosis and related tests. *R package version* **14** (2015).
126. Kassambara, A. (2023).
127. Lemon, J. Plotrix: A package in the red light district of R. *R.-N.* **6**, 8–12 (2006).
128. Kassambara, A. Factoextra: extract and visualize the results of multivariate data analyses. *R package version* **1** (2016).
129. Lê, S., Josse, J. & Husson, F. FactoMineR: an R package for multivariate analysis. *J. Stat. Softw.* **25**, 1–18 (2008).
130. Caron, C., McCullagh, E. A. & Bertolin, G. Sex-specific loss of mitochondrial membrane integrity and mass in the auditory brainstem of a mouse model of Fragile X syndrome. *bioRxiv*, 2024.2007. 2002.601649 (2024).
131. Collins, S., Sarzani, R. & Bordicchia, M. Coordinate control of adipose 'browning'and energy expenditure by β-adrenergic and natriuretic peptide signalling. *Int. J. Obes. Suppl.* **4**, S17–S20 (2014).
132. Kim, H., Park, S. J. & Jou, I. STAT6 in mitochondrial outer membrane impairs mitochondrial fusion by inhibiting MFN2 dimerization. *iScience* **25**, 104923 (2022).
133. Kauppinen, A., Suuronen, T., Ojala, J., Kaarniranta, K. & Salminen, A. Antagonistic crosstalk between NF-κB and SIRT1 in the regulation of inflammation and metabolic disorders. *Cell. Signal.* **25**, 1939–1948 (2013).
134. Li, Y. et al. SIRT1 inhibits inflammatory response partly through regulation of NLRP3 inflammasome in vascular endothelial cells. *Mol. Immunol.* **77**, 148–156 (2016).

Acknowledgements

We thank members of the Tovar, Aguilar-Salinas, Aguilar-Arnal, and Orozco-Solis laboratories for helpful discussions and insights, and M. Bustamante-Zepeda, MSc., J.R. Cervantes-Roldán, MSc, and N.A. Gutiérrez-Najera, PhD., for technical assistance. We also acknowledge L.E. Guillén-Pineda, L. Estrada, and A. Cruz-Lopez for their technical assistance with DEXA and clinical analyses; E.Y. García-Villegas and S.A. Cruz-Reyez for their assistance with participant recruitment and logistics; and A. Valencia, R. Mojica, D.J. Gutierrez, J.E. Frías and L. Alfaro from the Microarray Unit at Instituto Nacional de Medicina Genómica for the transcriptomics experiments. Work in the RO-S lab was supported by Consejo Nacional de Humanidades, Ciencias y Tecnologías (CONACHYT) (grant nos. FC 2016/2672 and FOSISS 272757) INMEGEN (09/2017/I) and the Secretaría de Educación Ciencia, Tecnología e Inovación de la Ciudad de México (SECTEI) (grant 228/2021). LA-A lab was funded by UNAM-DGAPA-PAPIIT (IN210619, IN208022), Human Frontiers Science Program (HFSP) (LIY000193/2017) and the CONACHYT grant FORDECYTPRONACES /15758/2020. LM-V was supported by postdoctoral fellowship 740445 from CONACHYT, a postdoctoral fellowship from DGAPA-UNAM and a L'Oréal-UNESCO-Mexican Academy of Sciences (AMC) Fellowship for Women in Science. IR-A, is a doctoral student from the Programa de Doctorado en Ciencias Biomédicas, Universidad Nacional Autónoma de México (UNAM) and was supported by a graduate scholarship from CONACHYT (462646/574737). RV-L is a doctoral student from the Posgrado en Ciencias Bioquímicas (UNAM) and was supported by a graduate scholarship from CONACHYT, IS-R was supported by postdoctoral fellowship 350180 from CONACHYT.

Author contributions

R.O.-S., C.A.-S., I.C.-B., L.O., Conceived and designed the study. I.R.-A., R.V.-L., L.M.-V., I.S.-R., performed experiments and analyzed the data, T.L.V.-R. and J.M.-M., obtained participants biopsies and clinical data, I.R.-A. and L.G.N. performed OCR experiment's, R.O.-S., L.A.-A., I.R.-A., R.V.-L., L.M.-V., analyzed and interpreted data. M.C.R., L.O., L.A.-A., L.G.N., A.T., I.C.-B. and C.A.-S. provided equipment and reagents. I.R.-A., R.V.-L. and R.O.-S. wrote the manuscript. All authors reviewed the manuscript.

Competing interests
The authors declare no competing interest.

Ethics statement
This study was conducted in accordance with the principles of the Declaration of Helsinki. The research protocol was reviewed and approved by the Ethics Committees of the Instituto Nacional de Medicina Genómica and the Instituto Nacional de Ciencias Médicas y Nutrición Salvador Zubirán. All subjects were informed about the purpose and procedures of the study and signed an informed consent to participate. All ethical regulations relevant to human research participants were followed.

Additional information
Supplementary information The online version contains supplementary material available at https://doi.org/10.1038/s42003-025-07709-5.

Correspondence and requests for materials should be addressed to Ricardo Orozco-Solis.

Peer review information *Communications Biology* thanks the anonymous reviewers for their contribution to the peer review of this work. Primary Handling Editors: Gabriela Da Silva Xavier and Dario Ummarino. A peer review file is available.